PI3P dependent regulation of cell size and autophagy by phosphatidylinositol 5-phosphate 4-kinase

Avishek Ghosh, Aishwarya Venugopal, Dhananjay Shinde, Sanjeev Sharma, Meera Krishnan, Swarna Mathre, Harini Krishnan and Padinjat Raghu

National Centre for Biological Sciences, TIFR-GKVK Campus, Bellary Road, Bangalore 560065, India.

*Correspondence: praghu@ncbs.res.in

Tel: +91-80-23666102

Abstract

Phosphatidylinositol 3-phosphate (PI3P) and Phosphatidylinositol 5-phosphate (PI5P) are low abundant phosphoinositides crucial for key cellular events such as endosomal trafficking and autophagy. Phosphatidylinositol 5-phosphate 4-kinase (PIP4K) is an enzyme that regulates PI5P *in vivo* but can act on both PI5P and PI3P, *in vitro*. In this study, we report a novel role for PIP4K in regulating PI3P levels in *Drosophila* tissues. Loss-of-function mutants of the only PIP4K gene in *Drosophila* (*dPIP4K*^{29}) show reduced cell size in larval salivary glands. We find that PI3P levels are elevated in *dPIP4K*^{29} tissues and that reverting PI3P levels back towards wild type, without changes in PI5P levels, can also rescue the reduced cell size phenotype. *dPIP4K*^{29} mutants also show an upregulation in autophagy and the reduced cell size can be reverted by decreasing Atg8a, that is required for autophagosome maturation. Lastly, increasing PI3P levels in wild type salivary glands can phenocopy the reduction in cell size and associated upregulation of autophagy seen in *dPIP4K*^{29}. Thus, our study reports for the first time, a role for a PIP4K-regulated PI3P pool in the control of autophagy and cell size regulation that may explain the reported role of PIP4K in regulating neurodegeneration and tumour growth.

53 ## Introduction

54 The organization of membranes in eukaryotic cells is regulated by signalling mechanisms that
55 couple ongoing stimuli to sub-cellular transport mechanisms. Several signalling molecules
56 contribute to this process including proteins such as SNAREs and Rabs along with lipids.
57 Phosphoinositides are a class of signalling lipids found in all eukaryotes; they are
58 glycerophospholipids whose inositol headgroup can be phosphorylated on the 3rd, 4th or 5th
59 positions to generate molecules with signalling functions (Balla, 2013). In cells, phosphoinositides
60 are generated by the action of lipid kinases that are able to add phosphate groups to specific
61 positions on the inositol head group of specific substrates (Sasaki et al., 2009); thus the activity of
62 these lipid kinases and phosphatases is important to generate lipid signals on organelle membranes.
63 Phosphatidylinositol 5 phosphate 4-kinase (PIP4K) are one such class of lipid kinases that convert
64 phosphatidylinositol 5 phosphate (PI5P) into phosphatidylinositol 4,5 bisphosphate [PI(4,5)P_2]
65 (Clarke and Irvine, 2013; Rameh et al., 1997). Genetic analysis of *PIP4K* in various organisms
66 have demonstrated their importance in development and growth control (Gupta et al., 2013), cell
67 division (Emerling et al., 2013) immune cell function (Shim et al., 2016), metabolism (Lamia et
68 al., 2004) and neurological disorders (Al-Ramahi et al., 2017). At a cellular level, PIP4K have
69 been implicated in the control of plasma membrane receptor signalling (Sharma et al., 2019),
70 vesicular transport (Kamalesh et al., 2017), autophagy (Lundquist et al., 2018; Vicinanza et al.,
71 2015) and nuclear functions such as transcriptional control (Fiume et al., 2019). PI(4,5)P_2, the
72 product of PIP4K activity has many important functions in regulating cell physiology and
73 signalling (Kolay et al., 2016) and PI5P, the well-defined substrate of PIP4K has also been
74 implicated in regulating some sub-cellular processes (Hasegawa et al., 2017). However, despite
75 their importance in regulating several cellular processes and physiology, the biochemical reason for
76 the requirement of PIP4K in regulating these processes remain unclear.

77 When studied using biochemical activity assays *in vitro*, PIP4K shows very high activity on PI5P
78 to generate PI(4,5)P_2 (Ghosh et al., 2019; Rameh et al., 1997; Zhang et al., 1997). Coupled with
79 this, analysis of lipid levels following genetic depletion of PIP4K in various models have failed to
80 note appreciable reductions in PI(4,5)P_2 levels [reviewed in (Kolay et al., 2016)]. Rather, such
81 studies have reported an increase in the levels of the substrate, PI5P (Gupta et al., 2013; Jones et
82 al., 2006; Stijf-Bultsma et al., 2015) suggesting that the relevant biochemical function of the
83 enzyme is to regulate PI5P levels. Previous studies have noted that PIP4K depletion in *Drosophila*

84 photoreceptors (Kamalesh et al., 2017) leads to altered endocytic function and a role for PI5P in
85 regulating endocytosis has been proposed (Boal et al., 2015; Ramel et al., 2011). In mammalian
86 cells, PI5P has been proposed as a mediator of autophagy regulation by PIP4K (Al-Ramahi et al.,
87 2017; Lundquist et al., 2018; Vicinanza et al., 2015). PIP4K can also utilise PI3P as a substrate *in*
88 *vitro* (Ghosh et al., 2019; Gupta et al., 2013; Zhang et al., 1997), albeit with low efficiency;
89 however, the significance of this activity *in vivo* and the role of PIP4K, if any in regulating PI3P
90 levels *in vivo* is not known. PI3P is well known as a regulator of autophagy (Schink et al., 2016;
91 Wallroth and Haucke, 2018), a process that is reported to be altered on modulating PIP4K
92 function but the significance, if any, of PIP4K regulated pools of PI3P in these processes remains
93 unknown. PI3P formed at the phagophore membrane by Vps34, a class III PI3-kinase is important
94 for autophagy initiation by recruiting proteins like DFCP1, WIPI (Axe et al., 2008; Polson et al.,
95 2010). In the next step, the ATG16L1 complex, which includes the proteins ATG16L1, ATG5
96 and ATG12, is recruited to the pre-autophagosomal membranes (Dudley et al., 2019)and
97 Myotubularins, 3-phosphatase enzymes that have been reported to regulate autophagy by
98 regulating PI3P levels at autophagy initiation membranes (Taguchi-Atarashi et al., 2010; Vergne
99 et al., 2009; Zou et al., 2012). This raises the possibility that the reported regulation of autophagy
100 by PIP4K may arise from its ability to regulate PI3P levels at the autophagic membrane?

101

102 The *Drosophila* genome contains a single gene encoding PIP4K (*dPIP4K*). A loss-of-function allele
103 of dPIP4K (*dPIP4K*^{29}*)* results in altered growth and development, accumulation of the known
104 substrate PI5P and no reduction in PI(4,5)P_2 levels (Gupta et al., 2013). In *dPIP4K*^{29}, the size of
105 larval salivary gland cells is reduced and genetic reconstitution studies have demonstrated that the
106 kinase activity of dPIP4K, is required to support normal cell size (Mathre et al., 2019). Previous
107 work has shown that TORC1 signalling, a known regulator of cell size (Lloyd, 2013) and
108 autophagy (Nascimbeni et al., 2017), is reduced in *dPIP4K*^{29} (Gupta et al., 2013). Thus, while it
109 is clear that the kinase activity of dPIP4K is required for normal salivary gland cell size, the
110 biochemical basis for this requirement of enzyme activity is not known.

111

112 In this study, we show that in addition to the previously reported elevation of PI5P levels, PI3P
113 levels are also elevated in *dPIP4K*^{29} and this elevation in PI3P is dependent on the kinase activity
114 of dPIP4K. The reduced salivary gland cell size in *dPIP4K*^{29} could be rescued by the expression of

115 a PI3P specific 3-phosphatase, *Mtm* and this rescue was associated with a reversal of the elevated
116 PI3P but not PI5P levels. Interestingly, we observed that in larval salivary glands of *dPIP4K*^{29}, the
117 elevation in PI3P levels was associated with an upregulation in autophagy and the phenotype of
118 reduced cell size in *dPIP4K*^{29} could be reversed by down-regulating Atg8a, which functions
119 downstream to the formation of PI3P in the autophagy pathway. Elevation of PI3P levels in wild
120 type salivary glands by depletion of *Mtm* resulted in both a reduction in cell size and the enhanced
121 autophagy in salivary glands. Therefore, this study underscores a novel *in vivo* regulation of PI3P
122 levels by PIP4K in a multicellular organism leading to the control of cell size.

123

124 Results

125 *dPIP4K* does not regulate cell size through levels of its product PI(4,5)P_2

126 The kinase activity of dPIP4K is required for its ability to support salivary gland cell size (Figure 1A depicts
127 the conversion of PI5P to PI(4,5)P_2 by dPIP4K) (Mathre et al., 2019). Thus its ability to regulate cell size
128 may depend either on the elevated levels of its preferred substrate PI5P, or a shortfall in the pool of the
129 product PI(4,5)P_2 generated. Previous studies have identified a point mutation (A381E) in PIP4Kβ that
130 can switch its substrate specificity from PI5P to PI4P while still generating the same product PI(4,5)P_2
131 (Kunz et al., 2002). The corresponding point mutant version of hPIP4Kα has been used to distinguish
132 between phenotypes dependent on the PI(4,5)P_2 generated by PIP4K as opposed to PI5P metabolised by it
133 (Bulley et al., 2016). We generated a switch mutant version of human PIP4Kβ, hPIP4Kβ$^{[A381E]}$ that cannot
134 utilise PI5P as a substrate but can produce PI(4,5)P_2 using PI4P as a substrate (Kunz et al., 2002).
135 Expression of hPIP4Kβ$^{[A381E]}$ in the salivary glands of *dPIP4K*^{29} (AB1> hPIP4Kβ$^{[A381E]}$; *dPIP4K*^{29}) (Figure
136 S1A) did not rescue the reduced cell size whereas reconstitution with the wild type enzyme was able to do
137 so as previously reported (Figure S1Bi, quantified in Figure S1Bii, western blot in Figure S1A) (Mathre et
138 al., 2019). This observation suggests that the ability of dPIP4K to regulate cell size does not depend on the
139 pool of PI(4,5)P_2 that it generates and also that regulation of the levels of its substrate is likely to be the
140 relevant biochemical basis through which the enzyme supports cell size in salivary glands.

141

142 *Mtm* could be a candidate gene to modulate PI5P levels in *Drosophila*

143 Since PI5P is the preferred substrate of dPIP4K (Gupta et al., 2013), we sought to modulate PI5P levels to
144 assess the impact on cell size regulation. However, other biochemical players involved in PI5P regulation in
145 *Drosophila* are unknown so far. In mammals, PI5P levels are regulated by PIKFYVE, the type III PIP 5-

146 kinase that converts PI3P to PI(3,5)P_2 and PI to PI5P (Hasegawa et al., 2017; Shisheva, 2013). *Drosophila*
147 has a single PIKFYVE homologue (*CG6355*, here named *dFab1*) (Rusten et al., 2006); however, its
148 biochemical activity has not be tested (Figure 1A). We expressed mCherry tagged dFab1 in S2R+ cells,
149 immuno-precipitated it (Figure 1Ci) and analysed its ability to phosphorylate PI3P and PI, using a LC-
150 MS/MS based *in vitro* kinase activity assay for dFab1 (Figure 1B shows a schematic for the assay). We found
151 that the relative activity of dFab1 on synthetic PI3P was approximately 4 times greater than the activity on
152 synthetic PI (Figure 1Cii). Since dFab1 preferentially synthesizes PI(3,5)P_2 from PI3P, subsequent PI5P
153 generation would require the activity of a 3-phosphatase that can dephosphorylate PI(3,5)P_2. In mammals,
154 *in vitro* studies have revealed that lipid phosphatases of the myotubularin family have specific activity toward
155 PI3P and PI(3,5)P_2 (Figure 1A) (Laporte et al., 1996; Schaletzky et al., 2003; Walker et al., 2001). In most
156 higher order organisms, there are multiple myotubularin isoforms (Robinson and Dixon, 2006). It has been
157 suggested that *Drosophila* has six isoforms (Oppelt et al., 2013), but bioinformatic analysis using multiple
158 sequence alignment revealed that the conserved CX_5R catalytic motif is present in only 3 genes – *Mtm*,
159 *CG3632* and *CG3530* (Figure S1C). To identify the myotubularin that might generate PI5P from
160 PI(3,5)P_2, we designed a two-step *in vitro* LC-MS/MS based PI(3,5)P_2 3-phosphatase assay using *Drosophila*
161 S2R+ cell lysates as a source of enzyme (Figure 1D, details of the assay is mentioned in methods). Briefly,
162 deuterium labelled PI(3,5)P_2 [d5-PI(3,5)P_2] is incubated with cell lysate and the PI5P formed through the
163 action of a 3-phosphatase is converted, using ^{18}O-ATP to PI(4,5)P_2 of an unique mass owing to the
164 incorporated ^{18}O, and subsequently detected on a mass spectrometer (Figure 1D). We used a linked PI5P-
165 4-kinase assay to distinguish a 3-phosphatase activity generating PI5P from a 5-phosphatase activity
166 generating PI3P, from the cell lysates in the first step of the assay. Each of the 3-phosphatases (*Mtm*,
167 *CG3632* and *CG3530*) were depleted using dsRNA treatment (Worby et al., 2001) and the 3' phosphatase
168 activity of the lysates were measured. We noted more than 50% knockdown using dsRNA against *Mtm*,
169 *CG3632* and *CG3530* in S2R+ cells (Figure S1Di-iii). We observed that the d5-^{18}O-PIP_2 mole fraction [the
170 measure of PI(3,5)P_2 3-phosphatase activity] for *Mtm* downregulated lysates was significantly lower as
171 compared to control GFP dsRNA treated lysates (Figure 1E). However, we did not observe a significant
172 difference in activity of lysates downregulated for *CG3632* or *CG3530*. Therefore, Mtm is a 3-phosphatase
173 that could regulate PI5P synthesis in *Drosophila.*

174

175 ## *Drosophila* Mtm reverses the cell size defect of *dPIP4K^{29}* independent of PI5P levels

176 Based on the results of our *in vitro* results, we over-expressed *Mtm* in *dPIP4K^{29}* salivary glands to elevate
177 PI5P levels. If the reduced cell size in *dPIP4K^{29}* was linked to elevated PI5P levels, *Mtm* over-expression in
178 *dPIP4K^{29}* is expected to lead to a further reduction in cell size. Surprisingly, we observed that over-expression
179 of *Mtm* in the salivary glands of *dPIP4K^{29}* (*AB1> MtmGFP*; *dPIP4K^{29}*) resulted in a reversal of cell size as

180 compared to *dPIP4K*^{29} glands (Figure 2Ai, quantified in Figure 2Aii); over-expression of the enzyme in wild
181 type salivary glands did not affect cell size (Figure S2A).

182 Mtm is a 3-phosphatase that can act on PI3P to produce PI and PI(3,5)P_2 to produce PI5P. Previously, its
183 activity on PI(3,5)P_2 has been demonstrated using purified protein in an *in vitro* phosphate-release assay
184 (Velichkova et al., 2010). To understand the biochemical basis of the ability of over-expressed Mtm to
185 reverse cell size in *dPIP4K*^{29}, we tested the biochemical activity of Mtm from *Drosophila* larval extracts using
186 our two-step 3-phosphatase activity assay. Figure 2B shows expression of C-terminus GFP tagged Mtm
187 from larval lysates at molecular weights as predicted *in silico*. We found that overexpression of Mtm did not
188 result in a statistically significant increase in 3-phosphatase activity compared to controls (Figure 2C). To
189 confirm this result was not a result of C-terminal tagging leading to Mtm inactivation, we cloned an N-
190 terminus mCherry tagged Mtm and performed the 3-phosphatase assay using S2R+ cell lysates expressing
191 mCherry_Mtm (Figure S2Bi). It was observed that a N-terminally tagged Mtm was also not active on
192 PI(3,5)P_2 as compared to controls, much like its C-terminal GFP tagged counterpart (Figure S2Bii). These
193 findings suggest that the generation of PI5P from PI(3,5)P_2 by Mtm in *Drosophila* larvae is likely to be
194 minimal. We also measured the levels of PI5P from larval lipid extracts using a recently standardised LC-
195 MS/MS based PI5P mass assay (Ghosh et al., 2019), comparing larvae expressing Mtm in *dPIP4K*^{29} mutant
196 background with *dPIP4K*^{29}. We observed that the overexpression of Mtm did not alter the levels of PI5P in
197 *dPIP4K*^{29} (Figure 2D). Therefore, together we conclude that (a) Mtm cannot synthesise PI5P from
198 PI(3,5)P_2 *in vivo* in *Drosophila* and (b) Mtm expression rescued the cell size of *dPIP4K*^{29} without changing
199 the elevated PI5P levels. Therefore, we investigated PI5P independent mechanism that control cell size.

200

201 **Mtm reduces PI3P levels when over-expressed in *dPIP4K*^{29}**

202 Mtm has also been shown to dephosphorylate PI3P to generate PI *in vitro* (Velichkova et al., 2010). We
203 tested the activity of lysates expressing Mtm on synthetic PI3P using a LC-MS/MS based assay and found
204 that lysates with Mtm over-expression showed significantly higher PI3P 3-phosphatase activity compared
205 to control lysates (Figure 3A), raising the possibility that Mtm might be rescuing cell size in *dPIP4K*^{29}
206 through its PI3P 3-phosphatase activity.

207 Mtm activity can in principle change the levels of PI and PI3P; however since PI3P levels in cells are
208 substantially lower (<10%) of PI (Stephens et al., 1993), we analysed PI3P levels in relation to the ability
209 of Mtm overexpression to rescue the reduced cell size in *dPIP4K*^{29} salivary glands. Currently used methods
210 to quantify PI3P levels rely on radionuclide labelling techniques (Chicanne et al., 2012). We optimised a
211 previously used label-free LC-MS/MS based method to quantify PI3P levels from *Drosophila* larval lysates
212 [Fig 3B depicts a chromatogram derived from injecting wild type deacylated lipid samples] that allows the

213 chromatographic separation and quantification of PI3P levels (Kiefer et al., 2010). To test if the ability of
214 Mtm to dephosphorylate PI3P might be linked to its ability to reverse cell size in *dPIP4K*^{29}, we measured
215 PI3P levels in these genotypes. We observed that PI3P was significantly reduced in *dPIP4K*^{29} larvae
216 expressing Mtm compared to *dPIP4K*^{29} (Figure 3C). We also measured PI3P levels from larvae expressing
217 Mtm in an otherwise wild type background (Figure 3D) and found a modest reduction in the levels of
218 PI3P. These results highlight the potential for PI3P levels to be correlated to the phenotype of cell size
219 regulation in *Drosophila* salivary glands.

220

221 **dPIP4K regulates PI3P levels *in vivo***

222 Since reducing PI3P levels was correlated with cell size reversal in *dPIP4K*^{29} (Figure 2A and 3C), we
223 measured PI3P levels in *dPIP4K*^{29}. Interestingly, we observed that PI3P was elevated in *dPIP4K*^{29} larvae as
224 compared to controls (Figure 4A). In order to confirm this observation of elevated PI3P levels in *dPIP4K*^{29}
225 by an independent method, we devised an alternate assay to measure PI3P from larvae. Briefly, we developed
226 an *in vitro* lipid kinase reaction using purified mCherry::dFab1 to quantify PI3P from larval lipid extracts
227 using radionuclide labelling (schematic in Figure S4A). Figure 4B indicates the PI(3,5)P_2 spot on a TLC
228 formed from PI3P during the *in vitro* kinase reaction. Although lipid extracts from wild type and *dPIP4K*^{29}
229 larvae showed similar PI(3,5)P_2 spot intensities on the TLC (Figure 4B), normalisation of the PI(3,5)P_2 spot
230 intensity against total organic phosphate levels in each sample confirmed that the total PI3P levels were
231 higher in *dPIP4K*^{29} (Figure 4C) compared to controls. To confirm that the increase of PI3P in *dPIP4K*^{29}
232 was a result of the absence of PIP4K, we reconstituted wild type dPIP4K in *dPIP4K*^{29} and measured PI3P
233 (*Act5C> dPIP4KeGFP; dPIP4K*^{29}) and observed that the elevated PI3P in *dPIP4K*^{29} was reverted to normal,
234 indicating that dPIP4K can indeed regulate PI3P levels *in vivo* (Figure 4D). The catalytic activity of dPIP4K
235 is essential to maintain salivary gland cell size (Mathre et al., 2019). Therefore, to check whether this
236 catalytic activity was also necessary to control PI3P levels *in vivo*, we reconstituted *dPIP4K*^{29} with a
237 catalytically inactive dPIP4K (dPIP4K^{D271A}) and measured PI3P (*Act5C> dPIP4K*^{D271A}*; dPIP4K*^{29}); we found
238 that expressing catalytically dead dPIP4K^{D271A} could not significantly decrease the levels of PI3P in *dPIP4K*^{29}
239 (Figure 4E). These findings indicate that the catalytic activity of dPIP4K is required to regulate PI3P levels
240 *in vivo*.

241

242 **Regulation of PI3P by dPIP4K is unlikely to be via indirect mechanisms**

243 Although PI5P is the canonical *in vivo* substrate for dPIP4K, the enzyme can also use PI3P as a substrate
244 with low efficiency (Ghosh et al., 2019; Gupta et al., 2013), a feature conserved with mammalian PIP4Ks
245 (Zhang et al., 1997). In the context of our observation that PI3P levels are elevated in *dPIP4K*^{29}, dPIP4K

246 could regulate PI3P levels either through its ability to directly phosphorylate this lipid or indirectly via its
247 ability to regulate other enzymes that are established regulators of PI3P levels [e.g through negative
248 regulation of PI 3-kinase activity or through positive regulation of a 3-phosphatase that dephosphorylate
249 PI3P (Figure S4B)]. A reduction in 3-phosphatase activity on PI3P in *dPIP4K*^{29} could lead to accumulation
250 of PI3P. To test this possibility, the total 3-phosphatase activity of *dPIP4K*^{29} lysates was assessed. We did
251 not observe a reduction in 3-phosphatase activity that might explain the elevated PI3P levels. In fact, there
252 was an increase in response ratio (indicative of the 3-phosphatase activity on PI3P) in a 15 minutes *in vitro*
253 assay in mutant lysates as compared with wild type lysates (Figure 4F). In addition, we measured transcript
254 levels of three putative 3-phosphatases – *Mtm*, *CG3632* and *CG3530* and found that the transcript levels
255 of all the 3-phosphatases were unchanged in *dPIP4K*^{29} as compared to controls, although there was an overall
256 trend of decrease in all the genes (Figure 4G). PI3K59F activity could not be directly measured from larval
257 lysates; however, we measured the mRNA expression of the two known PI 3-kinase genes – *PI3K59F* and
258 *PI3K68D.* Although the transcript levels of *PI3K68D* was unchanged between *dPIP4K*^{29} and controls, we
259 observed that *PI3K59F* transcripts were in fact lower in *dPIP4K*^{29} compared to controls (Figure 4G). Thus,
260 it seems unlikely that upregulation of the aforementioned PI 3-kinases or downregulation of the 3-
261 phosphatases contributes to the increased PI3P levels in *dPIP4K*^{29}. These findings led us to conclude that
262 the regulation of PI3P levels by dPIP4K is unlikely via indirect mechanisms.

263

264 PIP4K regulates a non-endosomal PI3P pool in *Drosophila* salivary glands

265 The major source of PI3P generation in cells is the class III PI3-kinase called Vps34, whose *Drosophila*
266 ortholog is PI3K59F. PI3K59F is known to be functional at two locations in cells – namely the early
267 endosomal compartment and at multiple steps of autophagy pathway (Nascimbeni et al., 2017). In order
268 to understand the location at which PI3P is elevated in *dPIP4K*^{29}, we decided to restrict PI3K59F activity
269 to revert the increased PI3P levels at both locations of PI3K59F activity. Consequently, if PI3P at either or
270 both of these locations were relevant in regulating the cell size phenotype, we would achieve a reversal of
271 cell size by down-regulating PI3K59F in *dPIP4K*^{29} background. We down-regulated PI3K59F activity using
272 RNA interference (Figure S5A depicts the extent of *PI3K59F* transcript knockdown) in *dPIP4K*^{29}
273 background and indeed observed a reversal of cell size (Figure 5A); knockdown of *PI3K59F* in an otherwise
274 wild type background did not change cell size (Figure S5B). Further, measurement of PI3P from *dPIP4K*^{29}
275 larvae expressing PI3K59F RNAi showed a significant decrease in PI3P as compared to *dPIP4K*^{29} larvae
276 (Figure 5B).

277 To test if the early endosomal PI3P pool contributes to the reduced cell size in *dPIP4K*^{29}, we imaged the
278 tandem FYVE domain fused to mCherry (mCherry-2XFYVE), a reporter for endosomal PI3P, in salivary

279 glands of *dPIP4K*^{29} and compared it to wild type. The mCherry-2XFYVE probe revealed punctate structures
280 which were perinuclear (Figure 5Ci). Quantification of the number of punctae per unit area calculated for
281 the perinuclear sub-population showed no significant difference between wild type and *dPIP4K*^{29} salivary
282 glands (Figure 5Cii) although the probe was expressed at equal levels in both genotypes (Figure S5C). To
283 further validate if change of PI3P at the endosomal location in *dPIP4K*^{29} was correlated to the requirement
284 of dPIP4K to support cell size, we tagged dPIP4K with the tandem FYVE domain at the C-terminus end
285 of the protein (dPIP4K^{2XFYVE}) to target it to the PI3P enriched endosomal compartment and reconstituted
286 this in the background of *dPIP4K*^{29}. We did not observe a significant change in the cell size of *dPIP4K*^{29}
287 under these conditions suggesting that dPIP4K function is dispensable at this location (Figure 5D) for cell
288 size regulation.

289 The other sub-cellular location at which a Vps34-regulated PI3P pool is important, is the early
290 autophagosomal membranes. We were unable to directly measure the PI3P pool at autophagosomal
291 membranes. However, an increase in PI3P levels at this compartment would lead to an increase in the extent
292 of autophagy (Burman and Ktistakis, 2010) and can be assayed by an increase in the *Drosophila* ortholog of
293 microtubule-associated protein 1A/1B-light chain 3 (LC3) called Atg8a. We expressed mCherry::Atg8a in
294 salivary glands and the probe was expressed at equal levels in both genotypes (Figure S5D). Measurement
295 of the number of mCherry::Atg8a punctae showed a significant increase in *dPIP4K*^{29} glands compared to
296 controls (Figure 5Ei-ii), suggesting that the PI3P pool associated with the autophagy compartment is
297 upregulated in *dPIP4K*^{29}.

298

299 **PIP4K in *Drosophila* salivary glands affects bulk autophagy to affect cell size**

300 PI3P is formed by Vps34 and regulated by Atg1 mediated activation of the Vps34 Complex I components
301 Beclin-1 and Atg14, following which, lipidated Atg8a fuses with the formed omegasome membrane
302 containing PI3P to mature into autophagosomes (King et al., 2021). It has been demonstrated that
303 induction of autophagy by over-expressing Atg1 can cause a decrease in cell size of fat body cells in
304 *Drosophila* larvae (Scott et al., 2007). Likewise, in this study, we found that the over-expression of Atg1 in
305 the salivary glands of *Drosophila* larvae caused a drastic decrease in cell size (Figure S5E). Importantly,
306 downregulating Atg1 activity in *dPIP4K*^{29} could reverse the cell size phenotype in salivary glands while no
307 change was observed in otherwise wild type background, indicating that the autophagy pathway is
308 upregulated in *dPIP4K*^{29} (Figure S5Fi-ii). We reasoned that if the elevated PI3P in *dPIP4K*^{29} causes an
309 upregulation in autophagy leading to cell size reduction, then by down-regulating Atg8a, we would be able
310 to reverse the phenotype of cell size decrease. We indeed observed that down-regulation of Atg8a in
311 *dPIP4K*^{29} caused a reversal of the reduced cell size (Figure 5F), while there was no significant change in cell

312 size by down-regulation of Atg8a in otherwise wild type background (Figure S5G). Further, down-
313 regulation of Atg8a using the same RNAi line was able to decrease the number of mCherry::Atg8a in salivary
314 glands (Figure S5Hi-ii); the expression of the probe being equivalent between both genotypes (Figure S5I).

315

316 **PI3P regulates cell size in salivary glands**

317 We tested the effect of modulating PI3P levels in otherwise wild type salivary glands. Depletion of *Mtm*,
318 using an RNAi line has previously shown to increase PI3P levels in *Drosophila* (Jean et al., 2012; Velichkova
319 et al., 2010). Using qPCR analysis, we validated that the RNAi reagent causes specific down-regulation of
320 *Mtm* transcripts in *Drosophila* (Figure 6A). Interestingly, expressing Mtm RNAi in salivary glands caused a
321 significant decrease in cell size (Figure 6Bi and ii). Myotubularins are known to dimerize in cells and Mtm
322 harbours a C-terminal coiled-coil domain which can potentially aid in dimerization (Jean et al., 2012). We
323 observed a similar but smaller reduction in cell size when a catalytically dead version of Mtm (Mtm^{D402A}),
324 that is expected to act as dominant negative construct was expressed in salivary glands (Figure S6A). Further,
325 measurement of PI3P levels revealed a modest upregulation of PI3P levels when measured from larvae
326 expressing the Mtm RNAi (*da> Mtm RNAi*, Figure 6C). Therefore, Mtm inhibition in an otherwise
327 wildtype background can cause PI3P elevation and cell size decrease in *Drosophila*.

328 To understand if the reduction in cell size brought about by down-regulating Mtm in salivary glands causes
329 an upregulation of the autophagic pathway much like in *dPIP4K*^{29} mutants, we measured the number of
330 mCherry::Atg8a in salivary glands of Mtm RNAi (Figure 6Di). It was observed that there was a substantial
331 increase in the number of mCherry::Atg8a punctae as quantified in Figure 6Dii, although the expression of
332 the probe was expressed equivalent in both genotypes (Figure S6B). Interestingly, depleting Atg8a in salivary
333 glands also depleted of Mtm could partially rescue cell size as compared to glands where Mtm alone was
334 down-regulated (Figure 6E). These findings corroborate the relationship of increased PI3P levels to the
335 upregulation of autophagy which can eventually contribute to a decrease in cell size of salivary glands of
336 *Drosophila* larvae.

337

338 Discussion

339 Conceptually, the cellular function of any enzyme can be considered to arise from its ability to regulate the
340 levels of either the substrate or product. When PIP4K was originally described (Rameh et al., 1997), its
341 ability to generate the product $PI(4,5)P_2$ was recognised. However, $PI(4,5)P_2$, can also be synthesized from
342 phosphatidylinositol 4 phosphate (PI4P) by the activity of phosphatidylinositol 4 phosphate 5 kinase
343 (PIP5K) [reviewed in (Kolay et al., 2016)]. Since PI4P is ca.10 times more abundant than PI5P, loss of

344 PIP4K activity is unlikely to impact the overall levels of cellular PI(4,5)P_2. Consistent with this, knockout
345 of PIP4K does not reduce the overall level of PI(4,5)P_2 [(Gupta et al., 2013) discussed in (Kolay et al.,
346 2016)]. Further, a switch mutant version of PIP4K that can generate PI(4,5)P_2 from PI4P but not PI5P,
347 was unable to rescue the reduced cell size in *dPIP4K*^{29} implying that the biochemical basis of dPIP4K
348 function in supporting cell size is not its product PI(4,5)P_2. Rather, given that the kinase activity of the
349 enzyme is required for normal salivary gland cell size (Mathre et al., 2019), our findings imply that the
350 levels of the substrate are likely to be relevant. It was vital to be able to measure the levels of putative
351 substrates of PIP4K from *Drosophila* tissues and therefore, we developed a label-free LC-MS/MS based
352 methods to detect and quantify PI3P and PI5P. Previously researchers used more cumbersome radioactivity
353 based detection to measure PI3P and PI5P (Chicanne et al., 2012; Jones et al., 2013), however, new label-
354 free methods are being reported to quantify PIPs (Ghosh et al., 2019; Morioka et al., 2022). In this study,
355 we report the use of a label-free LC-MS/MS based method to measure PI3P levels *in vivo* from *Drosophila*
356 tissues for the first time. In future, this method can also be used to measure PI3P levels from tissues of other
357 model organisms to address key questions in PI3P biology.

358 Given that previous studies have identified PI5P as the substrate best utilised by PIP4K and that PI5P levels
359 are elevated in *dPIP4K*^{29}, we expected that the cell size phenotype will be mediated by PI5P levels. In the
360 course of this study, we found that (i) the expression of Mtm, a 3-phosphatase that is able to generate PI5P
361 *in vitro* from PI(3,5)P_2 rescued the reduced cell size in *dPIP4K*^{29}, (ii) The rescue of cell size in *dPIP4K*^{29} by
362 Mtm overexpression was not associated with a change in the levels of PI5P. These observations are not
363 consistent with a role for elevated PI5P levels in the reduced cell size phenotype of *dPIP4K*^{29}. Since PI3P
364 has also been shown to be a substrate of dPIP4K, albeit with less efficiency (Ghosh et al., 2019; Gupta et
365 al., 2013), we investigated PI3P levels and found that (i) PI3P levels were elevated in *dPIP4K*^{29}, (ii) were
366 reverted to wild type by reconstitution with a wild type dPIP4K transgene but not a kinase dead version,
367 (iii) the rescue of cell size in *dPIP4K*^{29} by expression of Mtm was associated with a reduction in the elevated
368 PI3P levels. Together, these findings strongly suggest that the elevated PI3P levels in *dPIP4K*^{29} underpin
369 the reduced salivary gland cell size. If elevated PI3P is a regulator of cell size, then elevation of PI3P levels
370 in wild type cells might also result in reduced cell size. Our observation that depletion of Mtm in a wildtype
371 background results in elevated PI3P levels and also reduced cell size supports this model. Overall, our data
372 supports a role for dPIP4K in the regulation of PI3P levels and cell size.

373 Interestingly, a recent study in MEFs grown in culture and downregulated of PIP4Kγ activity showed an
374 increase in PI3P and PI(3,5)P_2 levels along with an expected rise in PI5P levels (Al-Ramahi et al., 2017).
375 In mammals, the major route of synthesis of PI3P is through the action of a class III PI3-kinase called
376 Vps34. We observed that down-regulating PI3K59F, the ortholog of Vps34 in *Drosophila* reversed cell size

377 of *dPIP4K*^{29} salivary glands. These findings also identify PIP4K as a new regulator of PI3P levels along with
378 Vps34.

379 In spite of having specific stereo-chemistries, there are instances which demonstrate PI3P and PI5P to be
380 very similar to each other. The Fab1 (yeast orthologue of PIKfyve), YOTB, Vac 1 (vesicle transport
381 protein), and EEA1 (FYVE) domain has been used extensively for its lipid binding affinity for PI3P
382 (Gillooly et al., 2001). But NMR analysis revealed that FYVE domain show lesser albeit significant binding
383 affinity towards PI5P (Kutateladze et al., 1999). The Plant-Homeo-Domain (PHD) of ING2 protein,
384 which has been used in quite a few studies to probe PI5P location have revealed secondary avidities for PI3P
385 (Gozani et al., 2003). However, PIP4Kα has a less but significant *in vitro* kinase activity measured with
386 PI3P as substrate (Ghosh et al., 2019; Zhang et al., 1997). Consequently, purified *Drosophila* PIP4K also
387 shows a faint PI(3,4)P_2 spot measured through radioactive kinase assay indicating its 4-kinase activity on
388 PI3P (Gupta et al., 2013). However, due to the fold difference in *in vitro* activity between the two substrates,
389 it was never envisioned that PIP4K could regulate PI3P levels *in vivo*. Our results indicate a possibility
390 where the PIP4K can access a pool of PI3P *in vivo*, such that the enzyme achieves its optimal conditions for
391 a successful kinase reaction to metabolise PI3P.

392 What is the mechanism by which cell size is reduced in *dPIP4K*^{29}? It has been reported in several studies in
393 mammalian models that loss of PIP4K function is associated with an increase in either the initiation step
394 or flux of autophagy (Al-Ramahi et al., 2017; Lundquist et al., 2018; Vicinanza et al., 2015). Moreover, it
395 has been shown in human cells that PI5P can initiate autophagy and can even take over the function of
396 PI3P to initiate autophagy in wortmannin-treated cells (Vicinanza et al., 2015). We found that just by
397 altering PI3P levels without any change in PI5P levels, we could modify the phenotype of cell size of
398 *dPIP4K*^{29}. PI3P has been reported in primarily two cellular compartments, early endosomes and
399 autophagosomes. TORC1 activity is reported to be downregulated in *dPIP4K*^{29} (Gupta et al., 2013) and
400 consistent with the function of TORC1 in regulating autophagy, we found that levels of autophagy in
401 *dPIP4K*^{29} salivary gland cells was increased. Reducing PI3P levels by genetic knockdown of Vps34 (Class
402 III PI3K) reversed the reduced cell size phenotype in *dPIP4K*^{29} implying a role for Vps34 synthesized PI3P
403 in regulating cell size. Further, an early endosome specific dPIP4K construct could not revert the cell size
404 change of *dPIP4K*^{29}, indicating that the relevant pool of PI3P that regulates cell size is not at the early
405 endosome. Finally, inhibition of autophagy by down-regulation of Atg8a, a protein required downstream
406 of PI3P formation at the phagophore membrane during autophagosome biogenesis, in wild type results in
407 reduced cell size underscoring the requirement of normal levels of autophagy in controlling cell size in the
408 salivary gland. Additionally, we show that *Drosophila* Mtm also regulates cell size by downmodulating PI3P
409 levels and autophagy. Recent studies in *Drosophila* have identified a role for *CG3530/Mtmr6* in control of
410 basal autophagy in fat bodies (Allen et al., 2020; Manzéger et al., 2021). However, we do acknowledge that

411 Mtm downregulation does affect the endosomal PI3P pool as is reported earlier from the Kiger lab
412 (Velichkova et al., 2010). With the present data we cannot rule out an effect of endosomal PI3P in
413 contributing to cell size regulation in Mtm downregulation and perhaps the partial rescue of cell size by
414 down-regulating Atg8a explains this phenomenon (Figure 6E). Together our data provide compelling
415 evidence that the elevated levels of PI3P in *dPIP4K*^{29} induces enhanced autophagy leading to reduction in
416 cell size.

417 Materials and methods

418 ***Fly strains and stocks***

419 All experiments were performed with *Drosophila melanogaster* (hereafter referred to as *Drosophila*). Cultures
420 were reared on standard medium containing corn flour, sugar, yeast powder and agar along with
421 antibacterial and antifungal agents. Genetic crosses were set up with Gal4 background strains and
422 maintained at 25°C and 50% relative humidity (Brand and Perrimon, 1993). There was no internal
423 illumination within the incubator and the larvae of the correct genotype was selected at the 3rd instar
424 wandering stage using morphological criteria. *Drosophila* strains used were Oregon-R and *w*^{1118} (wild type
425 strain), *dPIP4K*^{29} (homozygous null mutant of dPIP4K made by Raghu lab), da-Gal4, Act5C-
426 Gal4/CyoGFP, AB1-Gal4, UAS hPIP4K2B/TM6Tb, UAS hPIP4K2B$^{[A381E]}$/TM6Tb, Mtm^{WT}GFP (Amy
427 Kiger, UCSD), Mtm-IR (#AK0246, Amy Kiger, UCSD), UAS dPIP4K^{WT}eGFP, UAS
428 dPIP4K$^{[D271A]}$(untagged), UAS PI3K59F RNAi (v100296, VDRC), Atg1 RNAi (44034, Bloomington),
429 Atg8a RNAi (34340, Bloomington), w; UAS-*mCherry:2XFYVE*^{2} (Amy Kiger, UCSD), UAS-mCherry-
430 Atg8a (37750, Bloomington).
431

432 ***S2R+R+ cells: culturing and transfection***

433 *Drosophila* S2R+R+ cells were cultured and maintained as mentioned earlier (Gupta et al., 2013).
434 Transient transfections for 48 hours were performed as mentioned previously (Mathre et al., 2019).
435 Primers for amplifying dsRNA template against *Drosophila* genes were selected from DRSC/TRiP
436 Functional Genomics Resources after confirming specificity of primers. A T7 RNA polymerase
437 promoter sequence (5'-TAATACGACTCACTATAGGGAGA-3') was added at the 5' end of the
438 primers for the T7 DNA dependent RNA polymerase to bind during *in vitro* transcription. The
439 dsRNA was synthesised using amplicons amplified from BDGP gold clones (Mtm: LD28822,
440 CG3632: LD11744 and CG3530: GH04637), purchased from DGRC. Following are the list of
441 primers used for the *in vitro* transcription of dsRNA:

442

Primer name	Sequence
Mtm dsRNA II F (DRSC36764)	5'-TAATACGACTCACTATAGGGAGAACTCGTCGCTGGACCAGTAT-3',
Mtm dsRNA II R (DRSC36764)	5'-TAATACGACTCACTATAGGGAGAATGCGTACAAGTAGGGGGAA-3'
CG3632 dsRNA II F (DRSC36821)	5'-TAATACGACTCACTATAGGGAGAACCATCGAGAAGAATGGACG-3'
CG3632 dsRNA II R (DRSC36821)	5'- TAATACGACTCACTATAGGGAGAATAGGAACGTGCCGAAGAGA- 3'
CG3530 dsRNA I F (DRSC36794)	5'-TAATACGACTCACTATAGGGAGAGCTCGATAGCAAGGAGCACT-3'
CG3530 dsRNA I R (DRSC36794)	5'- TAATACGACTCACTATAGGGAGACAGGAGCAGGTGGTTACGTT- 3'
GFP ds RNA F	5'- TAATACGACTCACTATAGGGATGGTGAGCAAGGGCGAGGAG - 3'
GFP ds RNA R	5'- TAATACGACTCACTATAGGGCTTGTACAGCTCGTCCATGCCG - 3'

443

444 **RNA extraction and qPCR analysis**

445 RNA was extracted from *Drosophila* S2R+R+ cells using TRIzol reagent (15596018, Life Technologies,
446 California, USA). Purified RNA was treated with amplification grade DNase I (18068015, Thermo Fisher
447 Scientific, California, USA). cDNA conversion was done using SuperScript II RNase H– Reverse
448 Transcriptase (18064014, Thermo Fisher Scientific) and random hexamers (N8080127, Thermo Fisher
449 Scientific). Quantitative PCR (Q-PCR) was performed using Power SybrGreen PCR master-mix (4367659,
450 Applied Biosystems, Warrington, UK) in an Applied Biosystem 7500 Fast Real Time PCR instrument.
451 Primers were designed at the exon-exon junctions following the parameters recommended for QPCR.
452 Transcript levels of the ribosomal protein 49 (RP49) were used for normalization across samples. Three
453 separate samples were collected from each treatment, and duplicate measures of each sample were conducted
454 to ensure the consistency of the data. The primers used were as follows:

Primer name	Sequence
Mtm Forward	5'-TAGCCAGCAGTTCAACAACG-3'
Mtm Reverse	5'-GTCTTGTGCTTGAGATCTTCGG-3'

CG3632 Forward	5'-TGAAAAGGTTCTTTGGCCAGC-3'
CG3632 Reverse	5'- CCATTGTGTCCGCTCTGTCT- 3'
CG3530 Forward	5'-TGGACACGTCGAGCTTCATC-3'
CG3530 Reverse	5'- TCGGTAGTAGGGGTTCAGCA- 3'
RP49 Forward	5'- CGGATCGATATGCTAAGCTGT - 3'
RP49 Reverse	5'- GCGCTTGTTCGATCCGTA - 3'
PI3K59F Forward	5'- ACCTATTTGCTGGGTGTGGG - 3'
PI3K59F Reverse	5'- CCTTGCTCAGCTTCATTGGC - 3'
PI3K68D Forward	5'- CGAGGACTACTCCCGTGTGA - 3'
PI3K68D Reverse	5'- GTTGCTGCATCTCCGCTGTA - 3'

455

456 ***Western blotting and immuno-precipitation***

457 **Westerns:** Salivary glands or larval samples were made exactly as mentioned in our previous work (Ghosh
458 et al., 2019; Mathre et al., 2019). Dilutions of antibodies used: 1:4000 for anti-tubulin (E7-c), (mouse)
459 from DSHB, 1:1000 for anti-mCherry antibody (Cat# PA5-34974) (Rabbit) from Thermo, 1:1000 for
460 anti-HA antibody (Cat# 2367S) (Mouse) from CST and Normal Rabbit IgG (sc-2027) from Santa Cruz.
461 **Immuno-precipitation:** About 2 million S2R+R+ cells were transfected for 48 hours and lysates were
462 prepared using 200 µl of same lysis buffer used for the preparation of protein samples for western blotting.
463 After lysis for 15 mins at 4 °C, the samples were spun down at 13000 X g for 10 mins to remove cellular
464 debris. 5% of the supernatant obtained was kept aside for input control; to the rest of the sample lysis buffer
465 was added to make up the volume to 1 mL. The volumes were split in two halves – one for IgG control and
466 the other for immune-precipitation. About 1.6 µg equivalent of antibody/normal rabbit IgG was used for
467 over-night incubation at 4 °C with continuous rotation. mCherry tagged *Drosophila* Fab1 complexes with
468 anti-mCherry antibody were precipitated by ~60 µl slurry of washed and blocked protein-G sepharose beads
469 (according to manufacturer's protocol, Sigma # GE17-0886-01) for 2 hours at 4 °C. The beads were then
470 washed with 0.1% TBST containing 0.1% 2-Mercaptoethanol, 0.1mM EGTA for two times and
471 resuspended in 100 µl of the same buffer and stored at 4 °C till kinase assay was performed.

472

473 ***Cell size measurements***

474 Salivary glands were dissected from wandering third instar larvae and fixed in 4% paraformaldehyde for 20
475 min at 4°C. Post fixation, glands were washed thrice with 1X Phosphate Buffered Saline (PBS) and
476 incubated in BODIPY™ FL C12-Sphingomyelin (Cat# D7711) for 3 hours at room temperature, following
477 which they were washed thrice in 1X PBS and stained with either DAPI (Thermo Fisher, cat# D1306) or
478 TOTO3 (Thermo Fisher, cat# T3604) for 10 mins at room temperature and washed with 1X PBS again.
479 About 2-3 glands per slide were then mounted in 70% glycerol and imaged. Imaging was done on Olympus

480 FV1000 or FV3000 Confocal microscope using a 10X objective. The images were then stitched into a 3D
481 projection using an ImageJ plugin. These reconstituted 3D z stacks were then analyzed for nuclei numbers
482 (for cell number) and volume of the whole gland using Volocity Software (version 5.5.1, Perkin Elmer Inc.).
483 The average cell size was calculated as the ratio of the average volume of the gland to the number of nuclei.
484

485 ***Atg8a punctae measurements***

486 Around 40 first instar larvae were picked and incubated per vial to control for crowding. Salivary glands
487 were dissected from wandering third instar larvae and fixed in 2.5% paraformaldehyde for 20 min at room
488 temperature. Post fixation, glands were washed twice with 1X PBS. Glands were mounted in 70% glycerol
489 and imaged on the same day. Imaging was done on an Olympus FV3000 Confocal microscope using a
490 60X objective. The 3D images were stitched to give one 2D image using Zproject in ImageJ. These 2D
491 images were then analysed for the number of punctae using the 3D object counter plugin in ImageJ. The
492 number of punctae were normalised to the area of the cell and plotted for the respective genotypes.

493

494 ***2xFYVE punctae measurements***

495 Salivary glands were dissected and imaged as described for the ATG8a punctae measurements. The 3D
496 images were stitched to give one 2D image using Zproject in ImageJ. The 2D images were then analysed
497 for the number of punctae (analysed using 3D object counter plugin in ImageJ). The number of punctae
498 were normalised to the area of the cell and plotted for the respective genotypes.

499

500 ***Lipid standards***

501 diC16-PI3P – Echelon P-3016*;* diC16-PI4P – Echelon P-4016; Avanti 850172 | rac-16:0 PI(3,5)P_2-d5
502 (Custom synthesised) ; 17: 0 20: 4 PI3P - Avanti LM-1900 ; 17: 0 20: 4 ; PI(4,5)P_2 - Avanti LM-1904.
503

504 ***Radioactivity based PI3P mass assay***

505 diC16-PI3P (Echelon) was mixed with 20 µM Phosphatidylserine (PS) (Sigma #P5660) and dried in *a*
506 centrifugal vacuum concentrator. For biological samples, PS was added to the organic phase obtained at the
507 end of the neomycin chromatography before drying. To the dried lipid extracts, 50 µl 10 mM Tris-HCl
508 pH 7.4 and 50 µl diethyl ether was added and the mixture was sonicated for 2 mins in a bath sonicator to
509 form lipid micelles. The tubes were centrifuged at 1000 X g to obtain a diethyl ether phase and vacuum
510 centrifuged for 2 mins to evaporate out the diethyl ether. At this time, the reaction was incubated on ice for
511 about 10 mins and 2X kinase assay buffer *(*100 mM Tris pH 7.4, 20 mM $MgCl_2$, 140 mM KCl, and 2 mM
512 EGTA and 10 µL immuno-precipitated dFab1 bead slurry was added. To this reaction, 10 µCi [γ-^{32}P] ATP

513 was added and incubated at 30 °C for 16 hours. Post 16 hours, the lipids were extracted from the reaction
514 as described earlier in a radioactive PI5P mass assay protocol (Jones et al., 2013).
515
516 *Thin layer Chromatography*
517 Extracted lipids were resuspended in chloroform and resolved by TLC (preactivated by heating at 90^0C for
518 1 hour) with a running solvent (45:35:8:2 chloroform: methanol: water:25% ammonia). Plates were air
519 dried and imaged on a Typhoon Variable Mode Imager (Amersham Biosciences).
520
521 *In Vitro dFab1 immunoprecipitate based Lipid 5-kinase assays*
522 600 picomoles of either 17:0 | 14:1 PI (Avanti # LM 1504) or 17:0 | 20:4 PI3P (Avanti # LM 1900) were
523 mixed with 20 µl of 0.5 (M) of Phosphatidylserine (PS) (P5660, Sigma) and dried in a centrifugal vacuum
524 concentrator. To this, 50 µl 10 mM Tris-HCl pH 7.4 was added and the mixture was sonicated for 3
525 minutes in a bath sonicator to form lipid micelles. At this time, the reaction was incubated on ice for ~ 10
526 minutes and 2X kinase assay buffer (100 mM Tris pH 7.4, 20 mM $MgCl_2$, 140 mM KCl, and 2 mM
527 EGTA and equal volumes of immunoprecipitated dFab1 was added. For LC-MS/MS based experiments
528 the kinase assay buffer contained 80 µM cold ATP (10519979001, Roche)). The rest of the procedure was
529 followed as mentioned in the following section.
530
531 *In Vitro larval lysate-based Lipid 3-phosphatase assays*
532 The assay conditions have been adopted from a previous study (Schaletzky et al., 2003). The phosphatase
533 assay comprises three parts- **(i) preparation of lysate:** third instar wandering larvae were collected in groups
534 of 5 and lysed in phosphatase lysis buffer containing 20 mM Tris-HCl (pH 7.4), 150 mM NaCl, 1% Triton
535 X-100 (v/v) and protease inhibitor cocktail (Roche), by incubating the resuspended mixture in ice for 15-
536 20 min. The larval carcasses were removed by a brief spin for 5 mins at 1000 x g speed. Total protein was
537 estimated by Bradford's reagent and desired amount of lysate was used for the subsequent assay. **(ii) Lipid**
538 **phosphatase assay:** 600 picomoles of either 17:0 20:4 PI3P or d5-PI(3,5)P_2 lipid was mixed and dried
539 with 20 µl of 0.5 M bovine brain derived Phosphatidylserine (PS) (Sigma #P5660) followed by bath
540 sonication of the mixture in presence of 50 µl of 10 mM Tris-HCl (pH 7.4) for 3 min at maximum
541 amplitude. To this 50 µl of 2× phosphatase assay buffer (Schaletzky et al., 2003) and 10 µg total protein
542 equivalents of cell free lysate was added and the reaction was incubated for 15 min at 37 °C. The reaction
543 was quenched with 125 µl of 2.4 (N) HCl followed by lipid extraction described earlier (Jones et al., 2013).
544 Samples for the PI3P assay were processed according to section (iii). For the PI(3,5)P_2 phosphatase assay
545 the dried lipids from this step were resuspended in 20 µl of 0.5 M PS and dried. To this, 50 µl of 10 mM
546 Tris-HCl (pH 7.4) was added and bath sonicated for 3 min similar to the first step of the assay. At this step,
547 50 µl of 2× kinase buffer containing 80 µM O^{18} ATP (OLM-7858-PK, Cambridge Isotope laboratories,

548 Inc) and 1 μg of bacterial purified human PIP4Kα-GST was added and the reaction was incubated at 30
549 °C for 1 hour. This was followed by lipid extraction as described in the previous step. **(iii) Derivatization**
550 **of lipids and LC-MS/MS:** The organic phases were collected from the last step and dried and 50 μl of 2M
551 TMS-diazomethane (Acros #AC385330050) was added to each tube and vortexed gently for 10 min at
552 room temperature. The reaction was neutralized using 10 μl of glacial acetic acid. The samples were dried
553 in vacuo and 200 μl of methanol was used to reconstitute the sample to make it ready for injection for LC-
554 MS/MS analysis.

555

556 ***Lipid isolation for PI5P and PI3P measurements***

557 Lipids from larvae were isolated from 3 or 5 third instar wandering larvae for PI5P or PI3P measurements,
558 respectively. Total lipids were isolated and neomycin chromatography (for PI5P measurements only) was
559 performed as described earlier (Ghosh et al., 2019).

560

561 ***LC-MS/MS for in vitro assays and PI5P measurements***

562 The instrument operation was followed similar to the description in our previous methods work on PI5P
563 quantification (Ghosh et al., 2019). For *in vivo* lipid measurements, the samples were washed with post-
564 derivatisation wash step before injecting in mass spec. Samples were run on a hybrid triple quadrupole mass
565 spectrometer (Sciex 6500 Q-Trap or Sciex 5500 Q-Trap) connected to a Waters Acquity UPLC I class
566 system. Separation was performed on a ACQUITY UPLC Protein BEH C4, 300Å, 1.7 μm, 1 mm X 100
567 mm column [Product #186005590] using a 45% to 100% acetonitrile in water (with 0.1% formic acid)
568 gradient over 10 mins. MS/MS and LC conditions used were as described earlier (Ghosh et al., 2019).

569

570 ***Larval PI3P measurements***

571 We adopted a previously used method of deacylation of total lipids followed by detection by LC-MS/MS
572 using ion-paring based separation chemistry followed by detection using mass spec (Jeschke et al., 2015;
573 Kiefer et al., 2010). Using our conditions, we could not reproducibly separate the deacylated PI5P isomeric
574 peak from biological samples. But we could always separate deacylated PI3P from PI4P in these biological
575 samples (Figure 3B). Synthetic standards were used to determine the retention times of the individual
576 peaks. Figure S3A shows synthetic GroPI3P at Rt = 6.13 min and GroPI4P at Rt = 6.95 min. The Rt of
577 GroPI3P and GroPI4P was shifted in case of biological samples and in order to confirm the peaks were
578 representative of the corresponding analytes, we spiked synthetic GroPI3P into the biological sample of
579 Figure S3B. As expected, we observed a spike in the first peak, albeit at Rt = 7.65 min, without a significant
580 change in the second peak at Rt = 8.70 min, thus confirming that the first peak was indeed corresponding
581 to PI3P. Further, we also verified that GroPI3P can be linearly detected at a range of 30 - 3000 picograms

582 on column and GroPI4P can be linearly detected at a range of 30 - 4000 picograms on column (Figure S3C
583 and S3D). We determined that the Limit of detection (LOD) was 20 picograms on column for GroPI3P
584 and GroPI4P as concluded from Signal to Noise (S/N) being 30 and 24, respectively.

585 The following are the steps by which PI3P measurements were performed: **(i) Larval lipid extraction:** As
586 mentioned in previous section **(ii) lipid deacylation:** Dried lipid extracts were incubated with 1 mL of 25%
587 methylamine solution in water/methanol/n-butanol (43:46:11) at 60 °C for 1 hour followed by drying this
588 extract in vacuo (~ 3-4 hours). **(iii) fatty acid wash:** Next, the lipids were reconstituted in 40-50 µl MS-
589 grade water and to this an equal volume fatty acid extraction reagent (1-butanol/petroleum ether (40–60
590 °C boiling)/ethyl formate in a ratio of 20/4/1 (vol/vol/vol)) was added and vortexed for 2 mins. Following
591 this, the tubes were centrifuged for 5 mins at 1000 x g to obtain phase separation. The upper organic phase
592 was discarded, and the lower aqueous phase was processed for LC-MS/MS analysis.

593 **MRM values for commercial lipids used:**

Lipids	Parent ion	Daughter ion
d5-diC16-PI5P	938.5	556.5
d5-diC16-PI(3,5)P_2	1046.5	556.5
d5-diC16-^{18}O-PIP_2	1052.5	556.5
17:0| 20:4 PI3P	995.5	613.5
17:0| 20:4 PIP_2	1103.5	613.5
17:0|14:1 PI	809.4	535.4
17:0|14:1 PIP	917.4	535.4

594

595 *LC-MS/MS for deacylated PI3P measurements*

596 Deacylated PIPs (GroPI3P and GroPI4P) were run on a hybrid triple quadrupole mass spectrometer (Sciex
597 6500 Q-Trap) connected to a Waters Acquity UPLC I class system. Separation was performed on a
598 Phenomenex Synergi™ 2.5 µm Fusion-RP 100 Å, LC Column 100 x 2 mm, [Product # 00D-4423-B0]
599 maintained at 32°C during the run. Mobile phase A consisted of 4 mM DMHA and 5 mM acetic acid in
600 water, and mobile phase B consisted of 4 mM DMHA and 5 mM acetic acid in 100% methanol. Flow rate
601 was 0.2 mL/min.

602 The process of linear gradient elution was conducted as follows: 0–2 min (methanol, 3%), 2–5 min
603 (methanol, 7%), 5–8 min (methanol, 12%), and 8–9 min (methanol, 100%). For next 4 min, solvent B
604 was maintained at 100%. Then, equilibration was performed between 12.2 and 20.0 min using 3%
605 methanol. The injection volume and running time of each sample was 3.0 µL and 20.0 min, respectively.

606 Mass spectrometry data was acquired in multiple reaction monitoring (MRM) mode in negative polarity.
607 Quantification of PIPs was achieved with the MRM pair (Q1/Q3) m/z 413→259. Electrospray (ESI)
608 Voltage was at – 4200 V and TEM (Source Temperature) as 350 °C, DP (Declustering Potential) at -55,
609 EP (Entrance Potential) at -10, CE (Collision Energy) at -31, CXP (Collision cell Exit Potential) at -12.
610 Dwell time of 100 milliseconds was used for experiments with CAD value of -3, GS1 and GS2 at 25, CUR
611 (Curtain gas) at 40. Both Q1 and Q3 masses were scanned at unit mass resolution.

612

613 ***Total Organic Phosphate measurement***

614 500 µl flow-through obtained from the phosphoinositide binding step of neomycin chromatography was
615 used for the assay for measurements of PI5P. For PI3P measurements, 50 µl was obtained from the last step
616 of lipid extraction and stored separately in phosphate free glass tubes till assay was performed. The sample
617 was heated till drying in a dry heat bath at $90^{0}C$ in phosphate-free glass tubes (Cat# 14-962-26F). The rest
618 of the process was followed as described previously (Jones et al., 2013).

619

620 ***Software and data analysis***

621 Image analysis was performed by Fiji software (Open source). Mass spec data was acquired on Analyst®
622 1.6.2 software followed by data processing and visualisation using MultiQuant™ 3.0.1 software and
623 PeakView® Version 2.0., respectively. Chemical structures were drawn with ChemDraw® Version 16.0.1.4.
624 Illustrations were created with BioRender.com. All datasets were statistically analysed using MS-Excel
625 (Office 2016).

626

627 **Acknowledgements:** This work was supported by the Department of Atomic Energy, Government of
628 India, under Project Identification No. RTI 4006 and a Wellcome-DBT India Alliance Senior
629 Fellowship to PR (IA/S/14/2/501540). We thank the NCBS Imaging and Mass Spectrometry Facility
630 and the *Drosophila* facility for support.

631

632

633

634

635

636

637 **References**

638 Al-Ramahi, I., Giridharan, S.S.P., Chen, Y.C., Patnaik, S., Safren, N., Hasegawa, J., de Haro, M., Gee,
639 A.K.W., Titus, S.A., Jeong, H., et al. (2017). Inhibition of PIP4Kγ ameliorates the pathological effects of
640 mutant huntingtin protein. Elife.

641 Allen, E.A., Amato, C., Fortier, T.M., Velentzas, P., Wood, W., and Baehrecke, E.H. (2020). A conserved
642 myotubularin-related phosphatase regulates autophagy by maintaining autophagic flux. J. Cell Biol. *219*.

643 Axe, E.L., Walker, S.A., Manifava, M., Chandra, P., Roderick, H.L., Habermann, A., Griffiths, G., and
644 Ktistakis, N.T. (2008). Autophagosome formation from membrane compartments enriched in
645 phosphatidylinositol 3-phosphate and dynamically connected to the endoplasmic reticulum. J. Cell Biol.
646 *182*, 685–701.

647 Balla, T. (2013). Phosphoinositides: Tiny Lipids With Giant Impact on Cell Regulation. Physiol. Rev. *93*,
648 1019–1137.

649 Boal, F., Mansour, R., Gayral, M., Saland, E., Chicanne, G., Xuereb, J.M., Marcellin, M., Burlet-Schiltz,
650 O., Sansonetti, P.J., Payrastre, B., et al. (2015). TOM1 is a PI5P effector involved in the regulation of
651 endosomal maturation. J. Cell Sci. *128*, 815–827.

652 Brand, A.H., and Perrimon, N. (1993). Targeted gene expression as a means of altering cell fates and
653 generating dominant phenotypes. *415*, 401–415.

654 Bulley, S.J., Droubi, A., Clarke, J.H., Anderson, K.E., Stephens, L.R., Hawkins, P.T., and Irvine, R.F.
655 (2016). In B cells, phosphatidylinositol 5-phosphate 4-kinase–α synthesizes PI(4,5)P_2 to impact mTORC2
656 and Akt signaling. Proc. Natl. Acad. Sci. *113*, 10571–10576.

657 Burman, C., and Ktistakis, N.T. (2010). Regulation of autophagy by phosphatidylinositol 3-phosphate.
658 FEBS Lett. *584*, 1302–1312.

659 Chicanne, G., Severin, S., Boscheron, C., Terrisse, A.D., Gratacap, M.P., Gaits-Iacovoni, F., Tronchère,
660 H., and Payrastre, B. (2012). A novel mass assay to quantify the bioactive lipid PtdIns3P in various
661 biological samples. Biochem. J. *447*, 17–23.

662 Clarke, J.H., and Irvine, R.F. (2013). Evolutionarily conserved structural changes in phosphatidylinositol
663 5-phosphate 4-kinase (PI5P4K) isoforms are responsible for differences in enzyme activity and localization.
664 Biochem. J. *454*, 49–57.

665 Dudley, L.J., Cabodevilla, A.G., Makar, A.N., Sztacho, M., Michelberger, T., Marsh, J.A., Houston, D.R.,
666 Martens, S., Jiang, X., and Gammoh, N. (2019). Intrinsic lipid binding activity of ATG 16L1 supports
667 efficient membrane anchoring and autophagy . EMBO J. *38*, 1–16.

668 Emerling, B.M., Hurov, J.B., Poulogiannis, G., Tsukazawa, K.S., Choo-Wing, R., Wulf, G.M., Bell, E.L.,
669 Shim, H.S., Lamia, K.A., Rameh, L.E., et al. (2013). Depletion of a putatively druggable class of
670 phosphatidylinositol kinases inhibits growth of p53-Null tumors. Cell *155*, 844–857.

671 Fiume, R., Faenza, I., Sheth, B., Poli, A., Vidalle, M.C., Mazzetti, C., Abdul, S.H., Campagnoli, F.,
672 Fabbrini, M., Kimber, S.T., et al. (2019). Nuclear phosphoinositides: Their regulation and roles in nuclear
673 functions. Int. J. Mol. Sci. *20*, 1–20.

674 Ghosh, A., Sharma, S., Shinde, D., Ramya, V., and Raghu, P. (2019). A novel mass assay to measure
675 phosphatidylinositol-5-phosphate from cells and tissues. Biosci. Rep. *39*, 707604.

676 Gillooly, D.J., Simonsen, A., and Stenmark, H. (2001). Cellular functions of phosphatidylinositol 3-
677 phosphate and FYVE domain proteins. Biochem. J. *355*, 249–258.

678 Gozani, O., Karuman, P., Jones, D.R., Ivanov, D., Cha, J., Lugovskoy, A.A., Baird, C.L., Zhu, H., Field,
679 S.J., Lessnick, S.L., et al. (2003). The PHD finger of the chromatin-associated protein ING2 functions as
680 a nuclear phosphoinositide receptor. *114*, 99–111.

681 Gupta, A., Toscano, S., Trivedi, D., Jones, D.R., Mathre, S., Clarke, J.H., Divecha, N., and Raghu, P.
682 (2013). Phosphatidylinositol 5-phosphate 4-kinase (PIP4K) regulates TOR signaling and cell growth
683 during Drosophila development. Proc. Natl. Acad. Sci. *110*, 5963–5968.

684 Hasegawa, J., Strunk, B.S., and Weisman, L.S. (2017). PI5P and PI(3,5)P2: Minor, but essential
685 phosphoinositides. Cell Struct. Funct. *42*, 49–60.

686 Jean, S., Cox, S., Schmidt, E.J., Robinson, F.L., and Kiger, A. (2012). Sbf/MTMR13 coordinates PI(3)P
687 and Rab21 regulation in endocytic control of cellular remodeling. Mol. Biol. Cell *23*, 2723–2740.

688 Jeschke, A., Zehethofer, N., Lindner, B., Krupp, J., Schwudke, D., Haneburger, I., Jovic, M., Backer, J.M.,
689 Balla, T., Hilbi, H., et al. (2015). Phosphatidylinositol 4-phosphate and phosphatidylinositol 3-phosphate
690 regulate phagolysosome biogenesis. Proc. Natl. Acad. Sci. *112*, 201423456.

691 Jones, D.R., Bultsma, Y., Keune, W.J., Halstead, J.R., Elouarrat, D., Mohammed, S., Heck, A.J., D'Santos,
692 C.S., and Divecha, N. (2006). Nuclear PtdIns5P as a transducer of stress signaling: an in vivo role for
693 PIP4Kbeta. Mol. Cell *23*, 685–695.

694 Jones, D.R., Ramirez, I.B.-R., Lowe, M., and Divecha, N. (2013). Measurement of phosphoinositides in
695 the zebrafish Danio rerio. Nat. Protoc. *8*, 1058–1072.

696 Kamalesh, K., Trivedi, D., Toscano, S., Sharma, S., Kolay, S., and Raghu, P. (2017). Phosphatidylinositol
697 5-phosphate 4-kinase regulates early endosomal dynamics during clathrin-mediated endocytosis. J. Cell Sci.
698 *130*, 2119–2133.

699 Kiefer, S., Rogger, J., Melone, A., Mertz, A.C., Koryakina, A., Hamburger, M., and Küenzi, P. (2010).
700 Separation and detection of all phosphoinositide isomers by ESI-MS. J. Pharm. Biomed. Anal. *53*, 552–
701 558.

702 King, K.E., Losier, T.T., and Russell, R.C. (2021). Regulation of Autophagy Enzymes by Nutrient
703 Signaling. Trends Biochem. Sci. 1–14.

704 Kolay, S., Basu, U., and Raghu, P. (2016). Control of diverse subcellular processes by a single multi-
705 functional lipid phosphatidylinositol 4,5-bisphosphate [PI(4,5)P2]. Biochem. J. *473*, 1681–1692.

706 Kunz, J., Fuelling, A., Kolbe, L., and Anderson, R.A. (2002). Stereo-specific substrate recognition by
707 phosphatidylinositol phosphate kinases is swapped by changing a single amino acid residue. J Biol Chem
708 *277*, 5611-9.

709 Kutateladze, T.G., Ogburn, K.D., Watson, W.T., De Beer, T., Emr, S.D., Burd, C.G., and Overduin, M.
710 (1999). Phosphatidylinositol 3-Phosphate Recognition by the FYVE Domain The in vivo interactions
711 between FYVE domains and PtdIns(3)P are essential for the function of several pro- teins. For example,
712 EEA1 (human early endosome au. Mol. Cell *3*, 805–811.

713 Lamia, K.A., Peroni, O.D., Kim, Y.B., Rameh, L.E., Kahn, B.B., and Cantley, L.C. (2004). Increased
714 insulin sensitivity and reduced adiposity in phosphatidylinositol 5-phosphate 4-kinase beta-/- mice. Mol
715 Cell Biol *24*, 5080–5087.

716 Laporte, J., Hu, L.J., Kretz, C., Mandel, J.L., Kioschis, P., Coy, J.F., Klauck, S.M., Poustka, A., and Dahl,
717 N. (1996). A gene mutated in X-linked myotubular myopathy defines a new putative tyrosine phosphatase
718 family conserved in yeast. Nat. Genet. *13*, 175–182.

719 Lloyd, A.C. (2013). The regulation of cell size. Cell *154*, 1194–1205.

720 Lundquist, M.R., Goncalves, M.D., Loughran, R.M., Possik, E., Vijayaraghavan, T., Yang, A., Pauli, C.,
721 Ravi, A., Verma, A., Yang, Z., et al. (2018). Phosphatidylinositol-5-Phosphate 4-Kinases Regulate Cellular
722 Lipid Metabolism By Facilitating Autophagy. Mol. Cell *70*, 531-544.e9.

723 Manzéger, A., Tagscherer, K., Lőrincz, P., Szaker, H., Lukácsovich, T., Pilz, P., Kméczik, R., Csikós, G.,
724 Erdélyi, M., Sass, M., et al. (2021). Condition-dependent functional shift of two Drosophila Mtmr lipid
725 phosphatases in autophagy control. Autophagy *17*, 4010–4028.

726 Mathre, S., Reddy, K.B., Ramya, V., Krishnan, H., Ghosh, A., and Raghu, P. (2019). Functional analysis
727 of the biochemical activity of mammalian phosphatidylinositol 5 phosphate 4-kinase enzymes. Biosci. Rep.
728 *39*, BSR20182210.

729 Morioka, S., Nakanishi, H., Yamamoto, T., Hasegawa, J., Tokuda, E., Hikita, T., Sakihara, T., Kugii, Y.,

730 Oneyama, C., Yamazaki, M., et al. (2022). A mass spectrometric method for in-depth profiling of
731 phosphoinositide regioisomers and their disease-associated regulation. Nat. Commun. *13*, 1–9.

732 Nascimbeni, A.C., Codogno, P., and Morel, E. (2017). Phosphatidylinositol-3-phosphate in the regulation
733 of autophagy membrane dynamics. FEBS J. *284*, 1267–1278.

734 Oppelt, A., Lobert, V.H., Haglund, K., Mackey, A.M., Rameh, L.E., Liestøl, K., Schink, K.O., Pedersen,
735 N.M., Wenzel, E.M., Haugsten, E.M., et al. (2013). Production of phosphatidylinositol 5-phosphate via
736 PIKfyve and MTMR3 regulates cell migration. EMBO Rep. *14*, 57–64.

737 Polson, H.E.J., De Lartigue, J., Rigden, D.J., Reedijk, M., Urbé, S., Clague, M.J., and Tooze, S.A. (2010).
738 Mammalian Atg18 (WIPI2) localizes to omegasome-anchored phagophores and positively regulates LC3
739 lipidation. Autophagy *6*, 506–522.

740 Rameh, L., Tolias, K., Duckworth, B., and Cantley, L.C. (1997). A new pathway for synthesis of
741 phosphatidylinositol- 4,5-bisphosphate. Nature *390*, 192–196.

742 Ramel, D., Lagarrigue, F., Pons, V., Mounier, J., Dupuis-Coronas, S., Chicanne, G., Sansonetti, P.J., Gaits-
743 Iacovoni, F., Tronchere, H., and Payrastre, B. (2011). Shigella flexneri Infection Generates the Lipid PI5P
744 to Alter Endocytosis and Prevent Termination of EGFR Signaling. Sci. Signal. *4*, ra61–ra61.

745 Robinson, F.L., and Dixon, J.E. (2006). Myotubularin phosphatases: policing 3-phosphoinositides. *16*,
746 403–412.

747 Rusten, T.E., Rodahl, L.M., Pattni, K., Englund, C., Samakovlis, C., Dove, S., Brech, A., and Stenmark,
748 H. (2006). Fab1 phosphatidylinositol 3-phosphate 5-kinase controls trafficking but not silencing of
749 endocytosed receptors. Mol Biol Cell *17*, 3989–4001.

750 Sasaki, T., Takasuga, S., Sasaki, J., Kofuji, S., Eguchi, S., Yamazaki, M., and Suzuki, A. (2009). Mammalian
751 phosphoinositide kinases and phosphatases. Prog. Lipid Res. *48*, 307–343.

752 Schaletzky, J., Dove, S.K., Short, B., Lorenzo, O., Clague, M.J., and Barr, F. a (2003).
753 Phosphatidylinositol-5-phosphate activation and conserved substrate specificity of the myotubularin
754 phosphatidylinositol 3-phosphatases. Curr. Biol. *13*, 504–509.

755 Schink, K.O., Tan, K.-W., and Stenmark, H. (2016). Phosphoinositides in Control of Membrane
756 Dynamics. Annu. Rev. Cell Dev. Biol. *32*, 143–171.

757 Scott, R.C., Juhász, G., and Neufeld, T.P. (2007). Direct Induction of Autophagy by Atg1 Inhibits Cell
758 Growth and Induces Apoptotic Cell Death. Curr. Biol. *17*, 1–11.

759 Sharma, S., Mathre, S., Ramya, V., Shinde, D., and Raghu, P. (2019). Phosphatidylinositol 5 Phosphate

760 4-Kinase Regulates Plasma-Membrane PIP3 Turnover and Insulin Signaling. Cell Rep. *27*, 1979-1990.e7.

761 Shim, H., Wu, C., Ramsamooj, S., Bosch, K.N., Chen, Z., Emerling, B.M., Yun, J., Liu, H., Choo-Wing,
762 R., Yang, Z., et al. (2016). Deletion of the gene *Pip4k2c* , a novel phosphatidylinositol kinase, results in
763 hyperactivation of the immune system. Proc. Natl. Acad. Sci. *113*, 7596–7601.

764 Shisheva, A. (2013). PtdIns5P: News and views of its appearance, disappearance and deeds. Arch. Biochem.
765 Biophys.

766 Stephens, L.R., Jackson, T.R., and Hawkins, P.T. (1993). Agonist-stimulated synthesis of
767 phosphatidylinositol(3,4,5)-trisphosphate. A new intracellular signalling system? BBA - Mol. Cell Res.
768 *1179*, 27–75.

769 Stijf-Bultsma, Y., Sommer, L., Tauber, M., Baalbaki, M., Giardoglou, P., Jones, D.R., Gelato, K.A., van
770 Pelt, J., Shah, Z., Rahnamoun, H., et al. (2015). The Basal Transcription Complex Component TAF3
771 Transduces Changes in Nuclear Phosphoinositides into Transcriptional Output. Mol. Cell *58*, 453–467.

772 Taguchi-Atarashi, N., Hamasaki, M., Matsunaga, K., Omori, H., Ktistakis, N.T., Yoshimori, T., and
773 Noda, T. (2010). Modulation of local Ptdins3P levels by the PI phosphatase MTMR3 regulates constitutive
774 autophagy. Traffic *11*, 468–478.

775 Velichkova, M., Juan, J., Kadandale, P., Jean, S., Ribeiro, I., Raman, V., Stefan, C., and Kiger, A.A. (2010).
776 Drosophila Mtm and class II PI3K coregulate a PI(3)P pool with cortical and endolysosomal functions. J.
777 Cell Biol. *190*, 407–425.

778 Vergne, I., Roberts, E., Elmaoued, R.A., Tosch, V., Delgado, M.A., Proikas-Cezanne, T., Laporte, J., and
779 Deretic, V. (2009). Control of autophagy initiation by phosphoinositide 3-phosphatase jumpy. EMBO J.
780 *28*, 2244–2258.

781 Vicinanza, M., Korolchuk, V.I., Ashkenazi, A., Puri, C., Menzies, F.M., Clarke, J.H., and Rubinsztein,
782 D.C. (2015). PI(5)P regulates autophagosome biogenesis. Mol. Cell *57*, 219–234.

783 Walker, D.M., Urbé, S., Dove, S.K., Tenza, D., Raposo, G., Clague, M.J., Urbe, S., Dove, S.K., Tenza,
784 D., Raposo, G., et al. (2001). Characterization of MTMR3. an inositol lipid 3-phosphatase with novel
785 substrate specificity. Curr. Biol. *11*, 1600–1605.

786 Wallroth, A., and Haucke, V. (2018). Phosphoinositide conversion in endocytosis and the endolysosomal
787 system. J. Biol. Chem. *293*, 1526–1535.

788 Worby, C.A., Simonson-Leff, N., and Dixon, J.E. (2001). RNA interference of gene expression (RNAi) in
789 cultured Drosophila cells. Sci. STKE *2001*, 1–9.

790 Zhang, X., Loijens, J.C., Boronenkov, I. V, Parker, G.J., Norris, F.A., Chen, J., Thum, O., Prestwich,
791 G.D., Majerus, P.W., and Anderson, R.A. (1997). Phosphatidylinositol-4-phosphate 5-kinase isozymes
792 catalyze the synthesis of 3-phosphate-containing phosphatidylinositol signaling molecules. J. Biol. Chem.
793 *272*, 17756–17761.

794 Zou, J., Majerus, P.W., Wilson, D.B., Schrade, A., Chang, S.C., and Wilson, M.P. (2012). The role of
795 myotubularin-related phosphatases in the control of autophagy and programmed cell death. Adv. Biol.
796 Regul. *52*, 282–289.

797

798 Figure legends:

799 **Figure 1: Screening for a biochemical route to modulate PI5P levels in *Drosophila* as altering local**
800 **PI(4,5)P_2 couldn't change cell size of *dPIP4K*[29]**

801 (A) Schematic illustrating the putative enzymatic routes by which PI5P can be synthesised in *Drosophila*.
802 The activities of enzymes labelled in blue are known in mammalian cells, the activity of enzymes
803 labelled in red followed by "?" are still unknown in *Drosophila*, the activity of enzymes labelled in
804 green are known in *Drosophila*. The activity of PI5P to PI(4,5)P_2 is boxed and is linked to cell size
805 regulation in *Drosophila* (Mathre et al., 2019). PI: Phosphatidylinositol, PI3P: Phosphatidylinositol
806 3-phosphate, PI(3,5)P_2: Phosphatidylinositol 3,5 bisphosphate, PI5P: Phosphatidylinositol 5-
807 phosphate, PI(4,5)P_2: Phosphatidylinositol 4,5 bisphosphate.

808 (B) Schematic illustrating the LC-MS/MS based *in vitro* 5-kinase activity assay using S2R+ cells over-
809 expressing dFab1 enzyme to convert synthetic PI or PI3P to PI5P and PI(3,5)P_2, respectively.

810 (C) (i) Immunoprecipitated protein levels were analysed by Western blotting with an anti-mCherry
811 antibody. Control (IgG) was prepared without anti-mCherry. Input lane shows the correct size of
812 dFab1 protein ~230 kDa. UTC: Untransfected control.

813 (ii) *In vitro* kinase assay on synthetic PI and PI3P. Graph representing the Kinase activity (%) as the
814 normalised response ratio of "PI 5-kinase activity on PI" to "PI3P 5-kinase activity on PI3P" upon
815 enzymatic activity of immunoprecipitated mCherry::dFab1 on the respective substrates. Response ratio
816 of PI 5-kinase activity on PI is obtained from area under the curve (AUC) of 17:0 14:1 PI5P
817 (Product)/17:0 14:1 PI (Substrate), Response ratio of PI3P 5-kinase activity on PI3P is obtained from
818 area under the curve (AUC) of 17:0 20:4 PI(3,5)P_2 (Product)/17:0 20:4 PI3P (Substrate) and is
819 represented as mean ± S.E.M. on addition of either negative control (no beads), Control (mCherry
820 beads) or dFab1 (mCherry::dFab1 beads). Number of immunoprecipitated samples = 2.

821 (D) Schematic illustrating the LC-MS/MS based *in vitro* $PI(3,5)P_2$ 3-phosphatase activity assay using
822 dsRNA treated S2R+ cells as enzyme source to convert synthetic $PI(3,5)P_2$ [d5-$PI(3,5)P_2$ to d5-^{18}O-
823 PIP_2] using a two-step reaction scheme.
824 (E) *In vitro* phosphatase assay on synthetic $PI(3,5)P_2$. Graph representing the 3-Phosphatase activity
825 (%) as the percent formation of d5-^{18}O-PIP_2 formed from starting d5-$PI(3,5)P_2$ as mean ± S.E.M.
826 on addition of either control (GFP ds RNA) or Mtm, CG3632, CG3530 ds RNA treated S2R+ cell
827 lysates. One way ANOVA with a post hoc Tukey's test shows p value = 0.003 between GFP and
828 Mtm ds RNA treated lysates, shows p value = 0.63 between GFP and CG3632 ds RNA treated
829 lysate and shows p value = 0.11 between GFP and CG3530 ds RNA treated lysates.

830 **Supporting Figure 1: Fab1 and Mtm can are potential PI5P modulating enzymes in *Drosophila***

831 (A) Protein levels between AB1Gal4/+ ; *dPIP4K*^{29} (Ctl), AB1 >hPIP4KB2::GFP ; *dPIP4K*^{29} and, AB1
832 >hPIP4KB2^{A381E}::GFP; *dPIP4K*^{29} from salivary glands of third instar wandering larvae seen on a
833 Western blot probed by GFP antibody. Both hPIP4KB2::GFP and hPIP4KB2^{A381E}::GFP migrates
834 ~75 kDa. Actin was used as the loading control.

835 (B)

836 (i) Representative confocal images of salivary glands from the genotypes a. *AB1/+ ; dPIP4K*^{29}
837 , b. *AB1>hPIP4Kβ; dPIP4K*^{29}, c. *AB1>hPIP4Kβ*$^{[A381E]}$*; dPIP4K*^{29}. Cell body is marked
838 majenta by BODIPY conjugated lipid dye, nucleus is marked by TOTO-3 shown in green.
839 Scale bar indicated at 100 μm.

840 (ii) Graph representing average cell size measurement (in μm^3) as mean ± S.E.M. of salivary
841 glands from wandering third instar larvae of *AB1/+; dPIP4K*^{29} (n = 9), *AB1>hPIP4Kβ;*
842 *dPIP4K*^{29} (n = 8), *AB1>hPIP4Kβ*$^{[A381E]}$*; dPIP4K*^{29} (n = 6). Sample size is represented on
843 individual bars. One way ANOVA with post hoc Tukey's test showed p value = 0.0002
844 between *AB1/+; dPIP4K*^{29} and *AB1>hPIP4Kβ; dPIP4K*^{29} and p value = 0.379 between
845 *AB1/+; dPIP4K*^{29} and *AB1>hPIP4Kβ*$^{[A381E]}$*; dPIP4K*^{29}.

846 (C) Multiple sequence alignment of the myotubularin phosphatase family proteins in *Drosophila* with
847 human myotubularins share a common signature phosphatase catalytic motif, the $C(X_5)R$ motif
848 (highlighted in red box) except *CG5026*, *CG14411*. The alignment was generated using clustalO
849 and representation is using Jalview. Conservation is shown in range of white to black, black being
850 most conserved.
851

852 (D) (i) qPCR measurements for mRNA levels of *Mtm, CG3632* and *CG3530* from either *GFP* ds RNA
853 (green) or *Mtm* ds RNA treated samples (majenta). Student's unpaired t-test showed p value =

854 0.009 between *GFP* ds RNA and *Mtm* ds RNA for *Mtm*, while p value = 0.36, p value = 0.46 for
855 genes *CG3632* and *CG3530*, respectively.

856 (ii) qPCR measurements for mRNA levels of *Mtm, CG3632* and *CG3530* from either *GFP* ds
857 RNA (green) or *CG3632* ds RNA treated samples (majenta). Student's unpaired t-test showed p
858 value = 0.02 between *GFP* ds RNA and *CG3632* ds RNA for *CG3632*, while p value = 0.29, p
859 value = 0.46 for genes *Mtm* and *CG3530*, respectively.

860 (iii) qPCR measurements for mRNA levels of *Mtm, CG3632* and *CG3530* from either *GFP* ds
861 RNA (green) or *CG3530* ds RNA treated samples (majenta). Student's unpaired t-test showed p
862 value = 0.0008 between *GFP* ds RNA and *CG3530* ds RNA for *CG3530*, while p value = 0.97, p
863 value = 0.31 for genes *Mtm* and *CG3632*, respectively.

864 **Figure 2: *Drosophila* Mtm rescues the cell size defect of *dPIP4K*^{29} independent of PI5P levels**

865 (A) (i) Representative confocal images of salivary glands from the genotypes a. *AB1/+ ; dPIP4K*^{29},
866 b. *AB1*>Mtm^{WT}GFP *; dPIP4K*^{29}. Cell body is marked majenta by BODIPY conjugated lipid dye,
867 nucleus is marked by TOTO-3 shown in green. Scale bar indicated at 50 μm.

868 (ii) Graph representing average cell size measurement (in percentage) as mean ± S.E.M. of
869 salivary glands from wandering third instar larvae of *AB1/+ ; dPIP4K*^{29} (n = 8),
870 *AB1*>Mtm^{WT}GFP*; dPIP4K*^{29} (n = 8). Sample size is represented on individual bars.
871 Student's unpaired t-test with Welch correction showed p value = 0.003 between *AB1/+ ;*
872 *dPIP4K*^{29} and *AB1*>Mtm^{WT}GFP *; dPIP4K*^{29}.

873

874 (B) Protein levels between *daGal4*/+ (Ctl) and *da*> Mtm^{WT}GFP from third instar wandering larvae seen
875 on a Western blot probed by GFP antibody. Mtm^{WT}GFP migrates ~100 kDa. Tubulin was used as
876 the loading control.

877 (C) *In vitro* phosphatase assay on synthetic PI(3,5)P_2. Graph representing the formation of ^{18}O-PIP$_2$
878 formed from starting PI(3,5)P_2 as substrate represented as mean ± S.E.M. on addition of either
879 control (da/+) or da>Mtm_GFP lysates. Lysate samples n = 3, where each sample was made from
880 five third instar wandering larvae. Student's unpaired t-test with Welch correction showed p value
881 = 0.23.

882 (D) Graph representing Normalised PI5P levels which is total ^{18}O-PIP$_2$/peak area of 17:0 20:4 PI(4,5)P_2
883 (internal standard) normalised to organic phosphate value as mean ± S.E.M. of da/+ ; *dPIP4K*^{29}
884 (green) or da> Mtm^{WT}GFP, *dPIP4K*^{29} (majenta). Biological samples n = 3, where each sample was

885 made from five third instar wandering larvae. Unpaired t test with Welch's correction showed p
886 value = 0.7830 between da/+ ; *dPIP4K*^{29} and da> Mtm^{WT}GFP, *dPIP4K*^{29}.

887

888 **Supporting Figure 2: *Drosophila* Mtm rescues the cell size defect of *dPIP4K*^{29} independent of PI5P**
889 **levels**

890 (A) Graph representing average cell size measurement (in percentage) as mean ± S.E.M. of salivary
891 glands from wandering third instar larvae of *AB1*/+ (n = 8) and *AB1*>Mtm^{WT}GFP (n = 8). Sample
892 size is also represented by points on individual bars. Student's unpaired t-test with Welch correction
893 showed p value = 0.392.

894 (B) (i) Protein levels between lysates made from *Drosophila* S2R+ cells. Lanes from left: untransfected
895 control (UTC), mCherry vector and mCherry_Mtm observed on a Western blot probed by
896 mCherry antibody. mCherry_Mtm migrates ~100 kDa. Tubulin was used as the loading control.

897 (ii) *In vitro* phosphatase assay on synthetic PI(3,5)P_2. Graph representing the formation of ^{18}O-
898 PIP_2 formed from starting PI(3,5)P_2 as substrate represented as mean ± S.E.M. on addition of either
899 control (mCherry vector transfected lysates) or mCherry_Mtm lysates. Lysate samples n = 3, where
900 each sample was made from five third instar wandering larvae. Student's unpaired t-test with Welch
901 correction showed p value = 0.696.

902

903 **Figure 3: Mtm reduces PI3P levels when over-expressed in *dPIP4K*^{29}**

904 (A) *In vitro* phosphatase assay on synthetic PI3P. Graph representing the response ratio of 17:0 20:4
905 PI (Product)/17:0 20:4 PI3P (Substrate) formed as mean ± S.E.M. on addition of either control
906 (da/+) or da>Mtm^{WT}GFP lysates. Lysate samples = 3, where each sample was made from five third
907 instar wandering larvae. Student's unpaired t-test with Welch correction showed p value = 0.007.

908 (B) Extracted ion chromatogram (XIC) of deacylated PI3P or GroPI3P (Glycerophosphoinositol 3-
909 phosphate) peak at Rt = 7.37 min, separated from deacylated PI4P or GroPI4P
910 (Glycerophosphoinositol 4-phosphate) peak at Rt = 9.12 min obtained from injecting wild type
911 larval lipid extract (details of sample preparation is discussed in methods).

912 (C) Graph representing Normalised PI3P levels which is the peak area of GroPI3P/ peak area of
913 GroPI4P normalised to organic phosphate value of total lipid extracts as mean ± S.E.M. of da/+ ;
914 *dPIP4K*^{29} (green) and da> Mtm^{WT}GFP, *dPIP4K*^{29} (majenta). Biological samples = 3, where each

915 sample was made from three third instar wandering larvae. Student's unpaired t-test with Welch
916 correction showed p value = 0.07.

917 (D) Graph representing Normalised PI3P levels which is the peak area of GroPI3P/ peak area of
918 GroPI4P normalised to organic phosphate value of total lipid extracts as mean ± S.E.M. of da/+
919 (green) and da> Mtm^{WT}GFP, (majenta). Biological samples = 3, where each sample was made from
920 three third instar wandering larvae. Student's unpaired t-test with Welch correction showed p value
921 = 0.13.

922

923

924

925 **Supporting Figure 3: Mtm reduces PI3P levels when over-expressed in *dPIP4K*^{29}**

926 (A) XIC obtained from a mixture of synthetic GroPI3P and GroPI4P standard mixture at 300
927 picograms on column eluting at Rt = 6.13 min and Rt = 6.95 min, respectively.

928 (B) XIC obtained from a biological sample spiked with 200 picograms of synthetic GroPI3P, eluting
929 at Rt = 7.65 min and GroPI4P eluting at Rt = 8.70 min, respectively. The area under the curve
930 (AUC) for GroPI3P changed by 29 times whereas the AUC of GroPI4P changed by 1.5 times,
931 indicating that the first peak obtained in biological samples is indeed GroPI3P.

932 (C) A dose–response curve of synthetic GroPI3P ranging from 30 to 3000 picograms on column. Y-
933 axis depicts intensity of GroPI3P (in cps) and X-axis represents the amount of GroPI3P loaded on
934 column. Equation: $y = 93.704x - 7243.1$; $R^2 = 0.9964$.

935 (D) A dose–response curve of synthetic GroPI4P ranging from 30 to 4000 picograms on column. Y-
936 axis depicts intensity of GroPI4P (in cps) and X-axis represents the amount of GroPI4P loaded on
937 column. Equation: $y = 212.49x - 505.82$; $R^2 = 0.9999$.

938

939 **Figure 4: dPIP4K regulates PI3P levels *in vivo***

940 (A) Graph representing Normalised PI3P levels which is the peak area of GroPI3P/ peak area of
941 GroPI4P normalised to organic phosphate value as mean ± S.E.M. of wild type (green) and
942 *dPIP4K*^{29} (majenta). Biological samples = 5, where each sample was made from five third instar
943 wandering larvae. Unpaired t-test with Welch correction showed p value = 0.008.

944 (B) Autoradiograph of TLC ran with lipid samples from *in vitro* PI3P mass assay using wild type (WT)
945 and *dPIP4K*^{29} lipid samples. The first two lanes from the left are obtained from mass assay reactions
946 using synthetic PI3P standard without or with addition of dFab1 enzyme, respectively. The origin
947 spot and PI(3,5)P_2 spots are marked.

948 (C) The graph represents normalised PI3P levels. Briefly, the spot marked as PI(3,5)P_2 on TLC in (B)
949 is obtained by converting PI3P in the samples using immunoprecipitated dFab1 in presence of
950 γ^{32}P-ATP are quantified using image analysis and then normalised to organic phosphate value
951 (indicated in blue embedded text under TLC) to obtain normalised PI3P levels. Biological samples
952 = 3, where each sample was made from five third instar wandering larvae. Student's unpaired t-test
953 with Welch correction showed p value = 0.036.

954 (D) Graph representing Normalised PI3P levels which is the peak area of GroPI3P/ peak area of
955 GroPI4P normalised to organic phosphate value of total lipid extracts as mean ± S.E.M. of
956 Act5C/+; *dPIP4K*^{29} (green), or Act5C> dPIP4K^{WT}GFP, *dPIP4K*^{29} (majenta). Biological samples =
957 5, where each sample was made from three third instar wandering larvae. Student's unpaired t-test
958 with Welch correction showed p value = 0.008.

959 (E) Graph representing Normalised PI3P levels which is the peak area of GroPI3P/ peak area of
960 GroPI4P normalised to organic phosphate value of total lipid extracts as mean ± S.E.M. of Act5C/+
961 ; *dPIP4K*^{29} (green) or Act5C> dPIP4K^{D271A}, *dPIP4K*^{29} (majenta). Biological samples = 6, where
962 each sample was made from three third instar wandering larvae. Student's unpaired t-test with
963 Welch correction showed p value = 0.818.

964 (F) *In vitro* phosphatase assay on synthetic PI3P. Graph representing the response ratio of 17:0 20:4
965 PI (Product)/17:0 20:4 PI3P (Substrate) formed as mean ± S.E.M. on addition of either wildtype
966 (WT) or *dPIP4K*^{29} lysates for either a 5 min or a 15 min reaction. Lysate samples = 3, where each
967 sample was made from five third instar wandering larvae. Multiple unpaired t-test showed p value
968 = 0.26 for 5 min time point and p value = 0.052.

969 (G) qPCR measurements for mRNA levels of *PI3K59F* and *PI3K68D* from either Wild type (green)
970 or *dPIP4K*^{29} (majenta). Student's unpaired t-test showed p value = 0.01 for *PI3K59F* and p value
971 = 0.58 for *PI3K68D*. qPCR measurements for mRNA levels of *Mtm, CG3632* and *CG3530* from
972 either Wild type (green) or *dPIP4K*^{29} (majenta). Student's unpaired t-test showed p value = 0.03
973 for *Mtm*, p value = 0.23 for *CG3632* and p value = 0.0006 for *CG3530*.

974

975 **Supporting Figure 4: *Drosophila* PIP4K regulates *in vivo* PI3P levels**

976 (A) Schematic illustrating the methodology to assay PI3P by a dFab1 mediated radioactivity-based
977 mass assay. dFab1 is purified from S2R+ cells by immunoprecipitation and used to convert PI3P
978 from total lipid extracts obtained from larvae in presence of Υ^{32}P-ATP to radiolabelled PI(3,5)P_2
979 product which is finally analysed using thin layer chromatography (TLC). A portion of the total
980 lipid extract is used for organic phosphate assay to normalise for sample size.

981 (B) Illustration depicting a model where the increased PI3P levels in *dPIP4K*^{29} can be explained by
982 either an activation of PI 3-kinase activity (green arrow) or an inhibition of PI3P 3-phosphatase
983 activity (red stubbed arrow).

984

985

986

987 **Figure 5: PIP4K in *Drosophila* salivary glands affects bulk autophagy to affect cell size**

988 (A) Graph representing average cell size measurement (in μm^3) as mean ± S.E.M. of salivary glands
989 from wandering third instar larvae of *AB1/+ ; dPIP4K*^{29} (n = 9), *AB1>PI3K59F* RNAi *; dPIP4K*^{29}
990 (n = 9). Sample size is represented on individual bars. Student's unpaired t-test with Welch
991 correction showed p value <0.0001.

992 (B) Graph representing Normalised PI3P levels which is the peak area of GroPI3P/ peak area of
993 GroPI4P normalised to organic phosphate value of total lipid extracts as mean ± S.E.M. of Act5C/+
994 ; *dPIP4K*^{29} (green), or Act5C> dPIP4K^{WT}GFP, *dPIP4K*^{29} (majenta). Biological samples = 5, where
995 each sample was made from five third instar wandering larvae. Student's unpaired t-test with Welch
996 correction showed p value = 0.011.

997 (C) (i) Representative confocal z-projections depicting a sub population of early endosomal
998 compartment using 2xFYVE-mCherry in the salivary glands from wandering third instar larvae of
999 *AB1*> 2xFYVE-mCherry and *AB1*> 2xFYVE-mCherry *; dPIP4K*^{29}. Scale bar indicated at 20 μm.

1000 (ii) Graph representing 2xFYVE punctae measurement in the salivary glands from wandering third
1001 instar larvae of *AB1*> 2xFYVEmCherry (N = 8, n=40) and *AB1*> 2xFYVEmCherry*; dPIP4K*^{29} (N
1002 =8, n = 40). Student's unpaired t-test with Welch correction showed p value = 0.4057

1003 (D) Graph representing average cell size measurement (in μm^3) as mean ± S.E.M. of salivary glands
1004 from wandering third instar larvae of *AB1/+ ; dPIP4K*^{29} (n = 8), *AB1>dPIP4K*^{2XFYVE} *; dPIP4K*^{29} (n
1005 = 8). Sample size is represented on individual bars. Student's unpaired t-test with Welch correction
1006 showed p value = 0.171.

1007 (E) **(i)** Representative confocal z-projections depicting autophagosomal levels using Atg8a-mCherry in
1008 the salivary glands from the wandering third instar larvae of *AB1>ATG8a-mCherry* and
1009 *AB1>ATG8a-mCherry; dPIP4K*^{29}. Scale bar indicated at 20 μm.

1010 **(ii)** Graph representing Atg8a punctae measurement in the salivary glands from wandering third
1011 instar larvae of *AB1>ATG8a-mCherry* (N = 10, n = 60) and *AB1>ATG8a-mCherry; dPIP4K*^{29} (N
1012 = 10, n = 62). Student's unpaired t-test with Welch correction showed p value <0.0001.

1013 (F) Graph representing average cell size measurement (in μm^3) as mean ± S.E.M. of salivary glands
1014 from wandering third instar larvae of *AB1/+ ; dPIP4K*^{29} (n = 9), *AB1>PI3K59F* RNAi *; dPIP4K*^{29}
1015 (n = 9). Sample size is represented on individual bars. Student's unpaired t-test with Welch
1016 correction showed p value <0.0001.

1017

1018 **Supporting Figure 5: PIP4K in *Drosophila* salivary glands affects bulk autophagy to affect cell size**

1019 (A) qPCR measurements for mRNA levels of *PI3K59F* and *PI3K68D* from either Control
1020 (Act5C/+, green) or Act5C > *PI3K59F* RNAi (majenta). Multiple t-test with post hoc Holm-
1021 Sidak's test showed p value < 0.0001 between *Act5C/+* and *Act5C> PI3K59F* RNAi for
1022 *PI3K59F* and p value = 0.62 between *Act5C/+* and *Act5C> PI3K59F* RNAi for *PI3K68D.*

1023 (B) Graph representing average cell size measurement (in μm^3) as mean ± S.E.M. of salivary glands
1024 from wandering third instar larvae of *AB1/+* (n = 12), *AB1>PI3K59F* RNAi (n = 9). Sample
1025 size is represented on individual bars. Student's unpaired t-test with Welch correction showed
1026 p value = 0.55.

1027 (C) Immunoblot from the salivary glands of wandering third instar larvae probed using mCherry
1028 antibody showing expression of 2xFYVE-mCherry in *AB1>2xFYVEmCherry* (control) and
1029 *AB1>2xFYVE-mCherry ; dPIP4K*^{29}. 2xFYVE-mCherry migrates ~50 kDa. Actin was used as
1030 the loading control. dPIP4K protein was checked in the samples to ascertain the mutant
1031 background.

1032 (D) Immunoblot from the salivary glands of wandering third instar larvae probed using mCherry
1033 antibody showing expression of Atg8a-mCherry in *AB1>ATG8amCherry* (control) and
1034 *AB1>ATG8amCherry ; dPIP4K*^{29}. Atg8a-mCherry migrates ~42 kDa. Tubulin was used as the
1035 loading control. dPIP4K protein was checked in the samples to ascertain the mutant
1036 background.

1037 (E) Graph representing average cell size measurement (in μm^3) as mean ± S.E.M. of salivary glands
1038 from wandering third instar larvae of *AB1*/+ (n = 3), *AB1*> *Atg1* (n = 2). Sample size is
1039 represented on individual bars. Statistical test not performed.

1040 (F) (i) Graph representing average cell size measurement (in μm^3) as mean ± S.E.M. of salivary
1041 glands from wandering third instar larvae of *AB1*/+ (n = 12), *AB1*> *Atg1* RNAi (n = 10).
1042 Sample size is represented on individual bars. Student's unpaired t-test with Welch correction
1043 showed p value = 0.92.

1044 (ii) Graph representing average cell size measurement (in μm^3) as mean ± S.E.M. of salivary
1045 glands from wandering third instar larvae of *AB1*/+ *; dPIP4K*^{29} (n = 11), *AB1*>*Atg1* RNAi
1046 *; dPIP4K*^{29} (n = 9). Sample size is represented on individual bars. Student's unpaired t-test
1047 with Welch correction showed p value <0.0001.

1048 (G) Graph representing average cell size measurement (in μm^3) as mean ± S.E.M. of salivary glands
1049 from wandering third instar larvae of *AB1*/+ (n = 9), *AB1*>*Atg8a* RNAi (n = 8). Sample size is
1050 represented on individual bars. Student's unpaired t-test with Welch correction showed p value
1051 = 0.67.

1052 (H) **(i)** Representative confocal z-projections depicting autophagosomal levels using Atg8a-
1053 mCherry in the salivary glands from the genotypes a. *AB1*>*ATG8a-mCherry* , b. *AB1*>*ATG8a-*
1054 *mCherry ; ATG8aRNAi* . Scale bar indicated at 20 µm.
1055 (ii) Graph representing Atg8a punctae measurement in the salivary glands from wandering
1056 third instar larvae of *AB1*>*ATG8a-mCherry* (N =8 , n =40) and *AB1*>*ATG8a-mCherry ;*
1057 *ATG8aRNAi* (N =8 ,n =40). Student's unpaired t-test with Welch correction showed p
1058 value = 0.0197.

1059 (I) Immunoblot from the salivary glands of wandering third instar larvae probed using mCherry
1060 antibody showing the expression of Atg8a-mCherry in *AB1*>*ATG8amCherry* (control) and
1061 *AB1*>*ATG8a-mCherry ; ATG8aRNAi*. Atg8a-mCherry migrates ~42 kDa. Actin was used as
1062 the loading control.

1063

1064 **Figure 6: PI3P regulates cell size in salivary glands**

1065 (A) qPCR measurements for mRNA levels of *mtm, CG3632 and CG3530* from either Control
1066 (*daGal4*/+, in green) or *da*> *Mtm* RNAi, in majenta. Multiple t-test with post hoc Holm-Sidak's
1067 test showed p value < 0.0001 between *daGal4*/+ and *da*> *Mtm* RNAi for *Mtm* and p value = 0.35

1068 between *daGal4*/+ and *da*> *Mtm* RNAi for *CG3632*, and p value = 0.04 between *daGal4*/+ and
1069 *da*> *Mtm* RNAi for *CG3530*.

1070 (B) (i) Representative confocal images of salivary glands from the genotypes a. *AB1Gal4*/+, b.
1071 *AB1*>*Mtm* RNAi. Cell body is marked majenta by BODIPY conjugated lipid dye, nucleus is
1072 marked by DAPI shown in green. Scale bar indicated at 50 μm.

1073 (ii) Graph representing average cell size measurement (in μm^3) as mean ± S.E.M. of salivary glands
1074 from wandering third instar larvae of *AB1Gal4*/+ (n = 7), *AB1*> *Mtm* RNAi (n = 7). Sample size is
1075 represented on individual bars. Student's unpaired t-test with Welch correction showed p value =
1076 0.0005.

1077 (C) Graph representing Normalised PI3P levels which is the peak area of GroPI3P/ peak area of
1078 GroPI4P normalised to organic phosphate value as mean ± S.E.M. of *da*/+ (green) and *da*> *Mtm*
1079 RNAi (majenta). Biological samples = 4, where each sample was made from five third instar
1080 wandering larvae. Student's unpaired t-test with Welch correction showed p value = 0.07.

1081 (D) (i) Graph representing Atg8a punctae measurement in the salivary glands from wandering third
1082 instar larvae of *AB1*>*ATG8a-mCherry* (N =7, n =40), *AB1*>*ATG8a-mCherry ; Mtm RNAi* (N =7 ,
1083 n =40). Student's unpaired t-test with Welch correction showed p value <0.0001.

1084 (ii) Representative confocal z-projections depicting autophagosomal levels using Atg8a-mCherry
1085 in the salivary glands from the genotypes a. *AB1*>*ATG8a-mCherry,* b. *AB1*>*ATG8a-mCherry; Mtm*
1086 *RNAi.* Scale bar indicated at 20 μm.

1087 (E) Graph representing average cell size measurement (in μm^3) as mean ± S.E.M. of salivary glands
1088 from wandering third instar larvae of *AB1*/+ (n = 11), *AB1*>*Mtm* RNAi (n = 8), *AB1*>*Mtm* RNAi,
1089 *Atg8a* RNAi (n = 12). Sample size is represented on individual bars. One way ANOVA with post
1090 hoc Tukey's test showed p value < 0.0001 between *AB1*/+ and *AB1*>*Mtm* RNAi and p value =
1091 0.0002 between *AB1*/+ *; dPIP4K*^{29} and *AB1*>*Mtm* RNAi, *Atg8a* RNAi.

1092 **Supporting Figure 6: PI3P regulates cell size in salivary glands**

1093 (A) Graph representing average cell size measurement (in μm^3) as mean ± S.E.M. of salivary glands
1094 from wandering third instar larvae of *AB1Gal4*/+ (n = 7), *AB1*> *Mtm* RNAi (n = 7). Sample size is
1095 represented on individual bars. Student's unpaired t-test with Welch correction showed p value =
1096 0.009.

1097 (B) Immunoblot from the salivary glands of wandering third instar larvae probed using mCherry
1098 antibody showing the expression of Atg8a-mCherry in *AB1*>*ATG8a-mCherry* (control) and

1099 *AB1>ATG8a-mCherry; Mtm RNAi*. Atg8a-mCherry migrates ~42 kDa. Tubulin was used as the
1100 loading control.

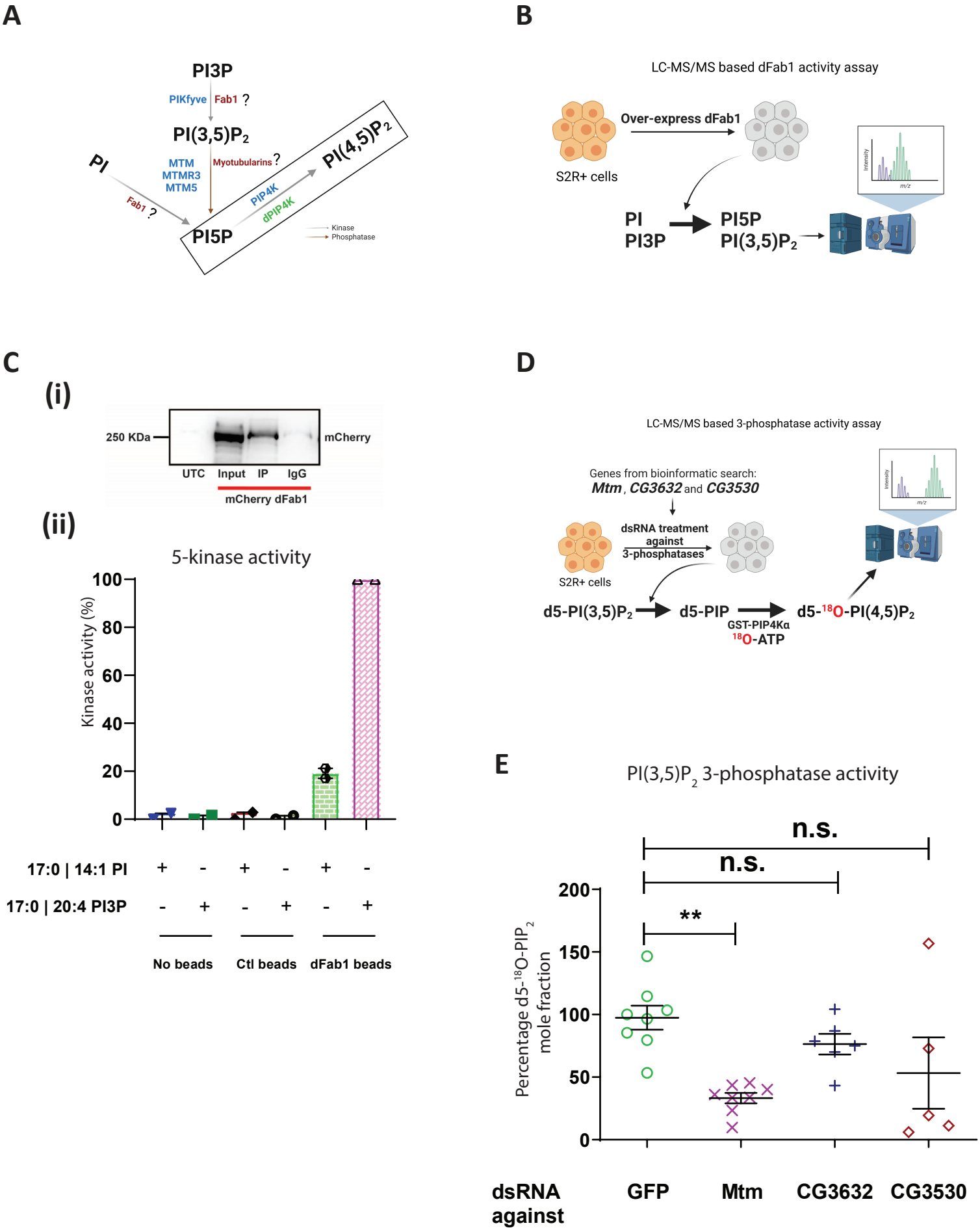

Ghosh et. al.,Figure 1

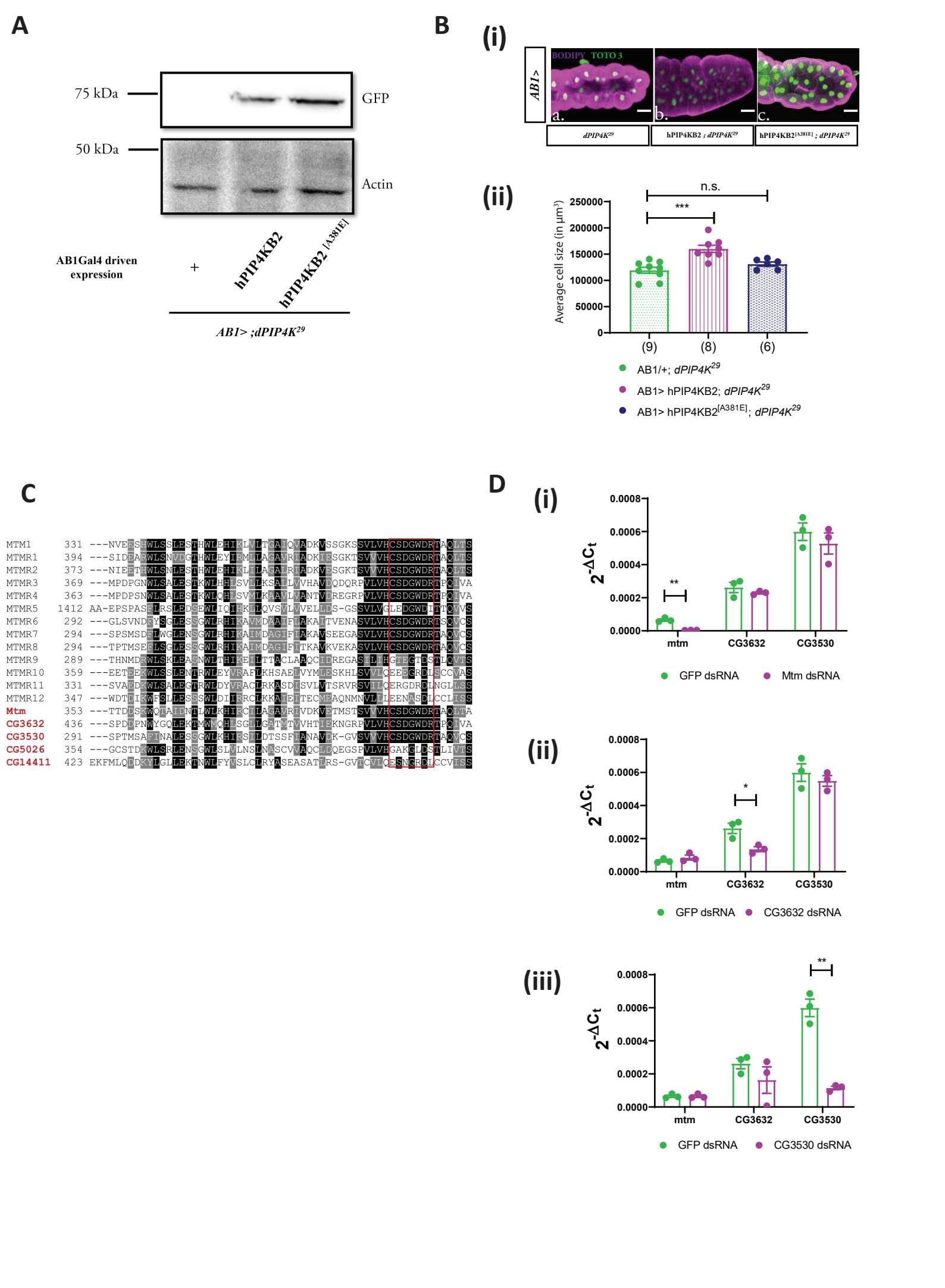

Ghosh et. al.,Figure S1

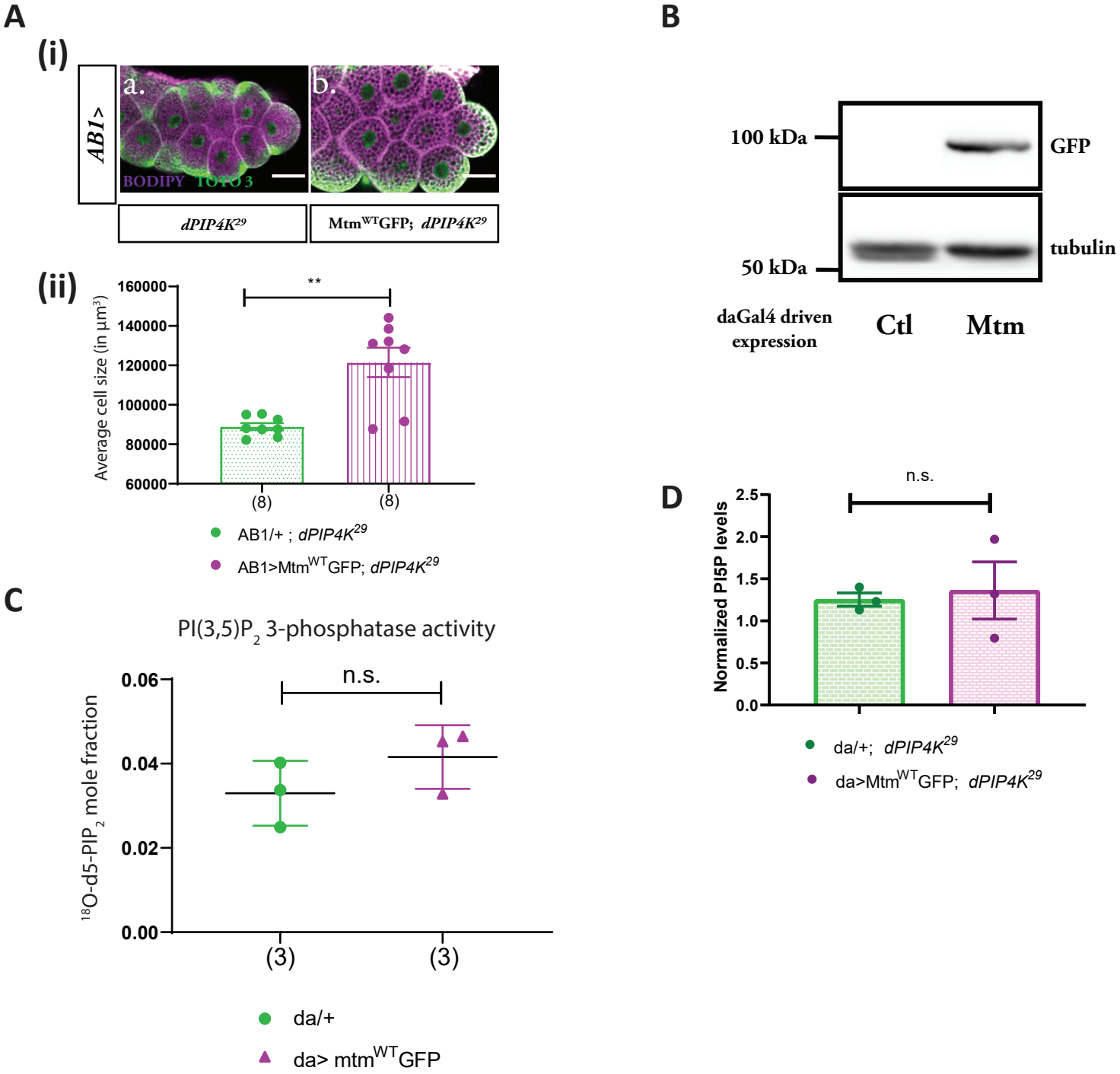

Ghosh et. al.,Figure 2

A

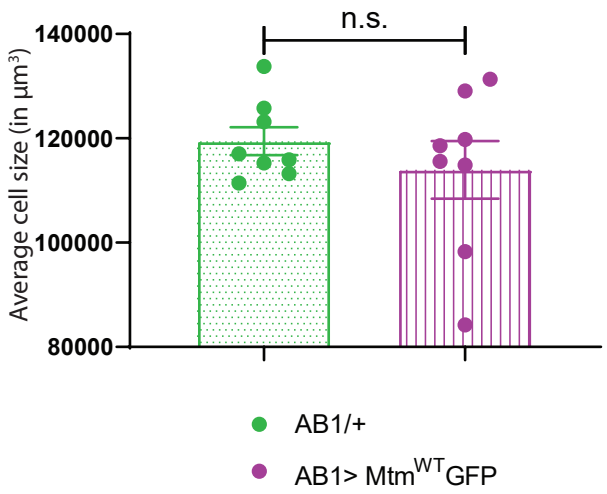

B

(i)

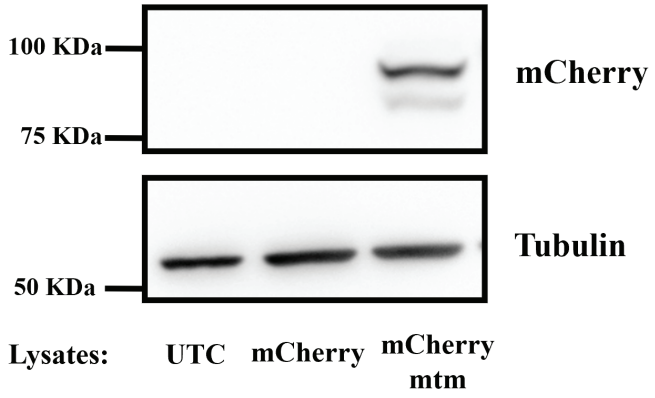

(ii)

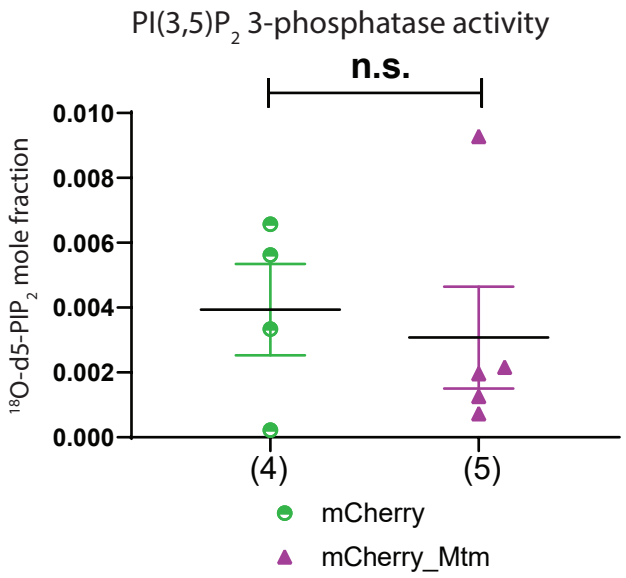

Ghosh et. al.,Figure S2

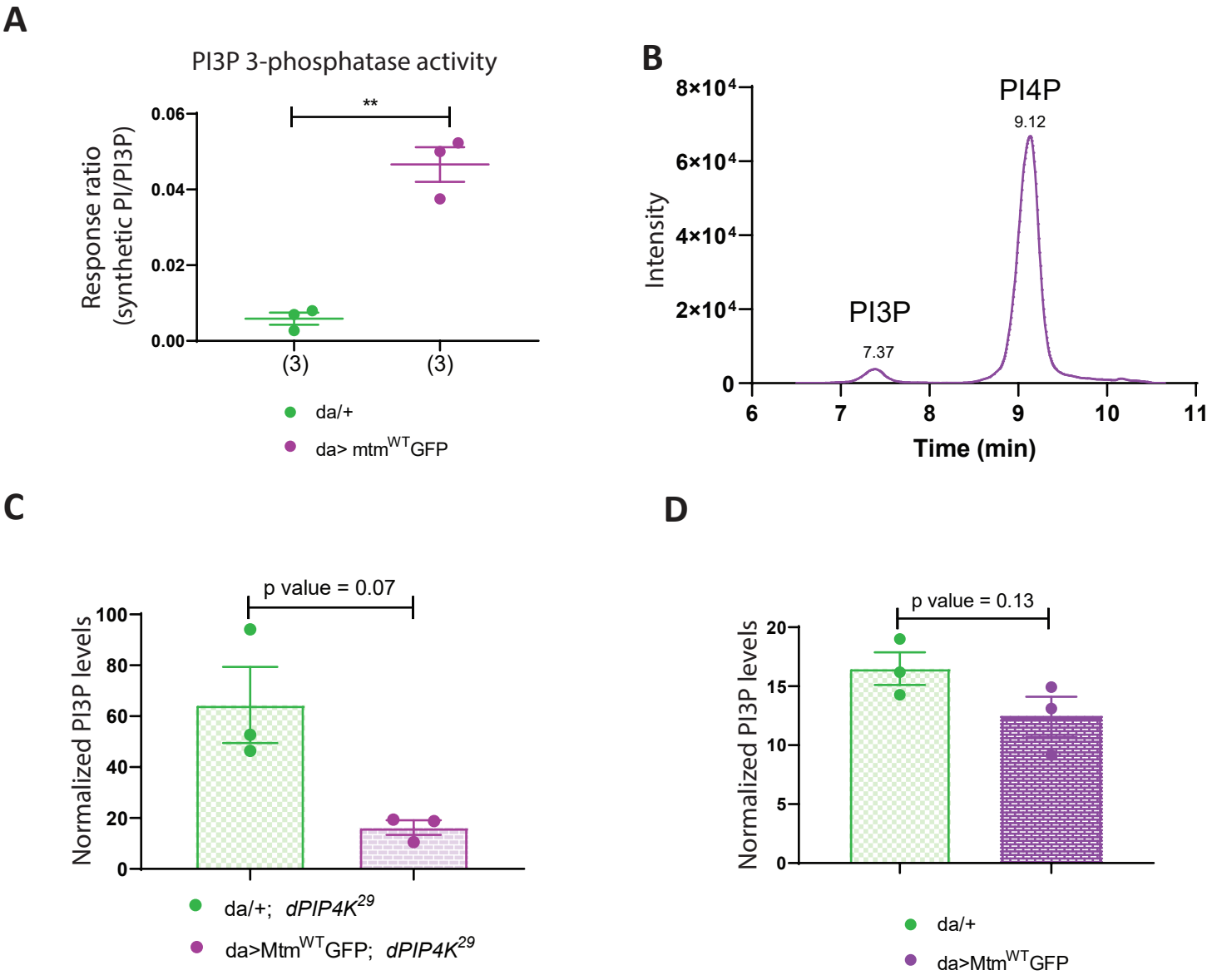

Ghosh et. al.,Figure 3

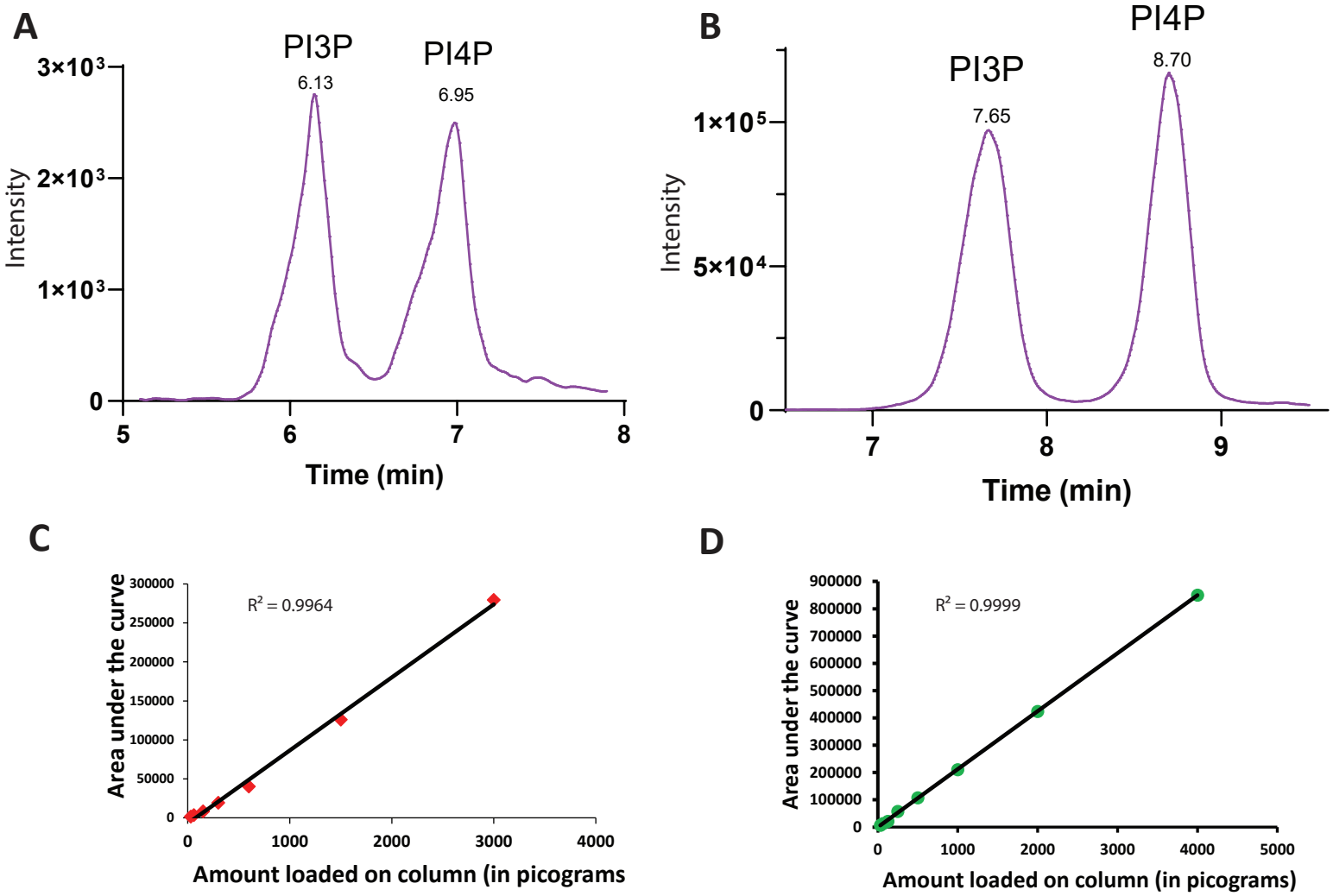

Ghosh et. al.,Figure S3

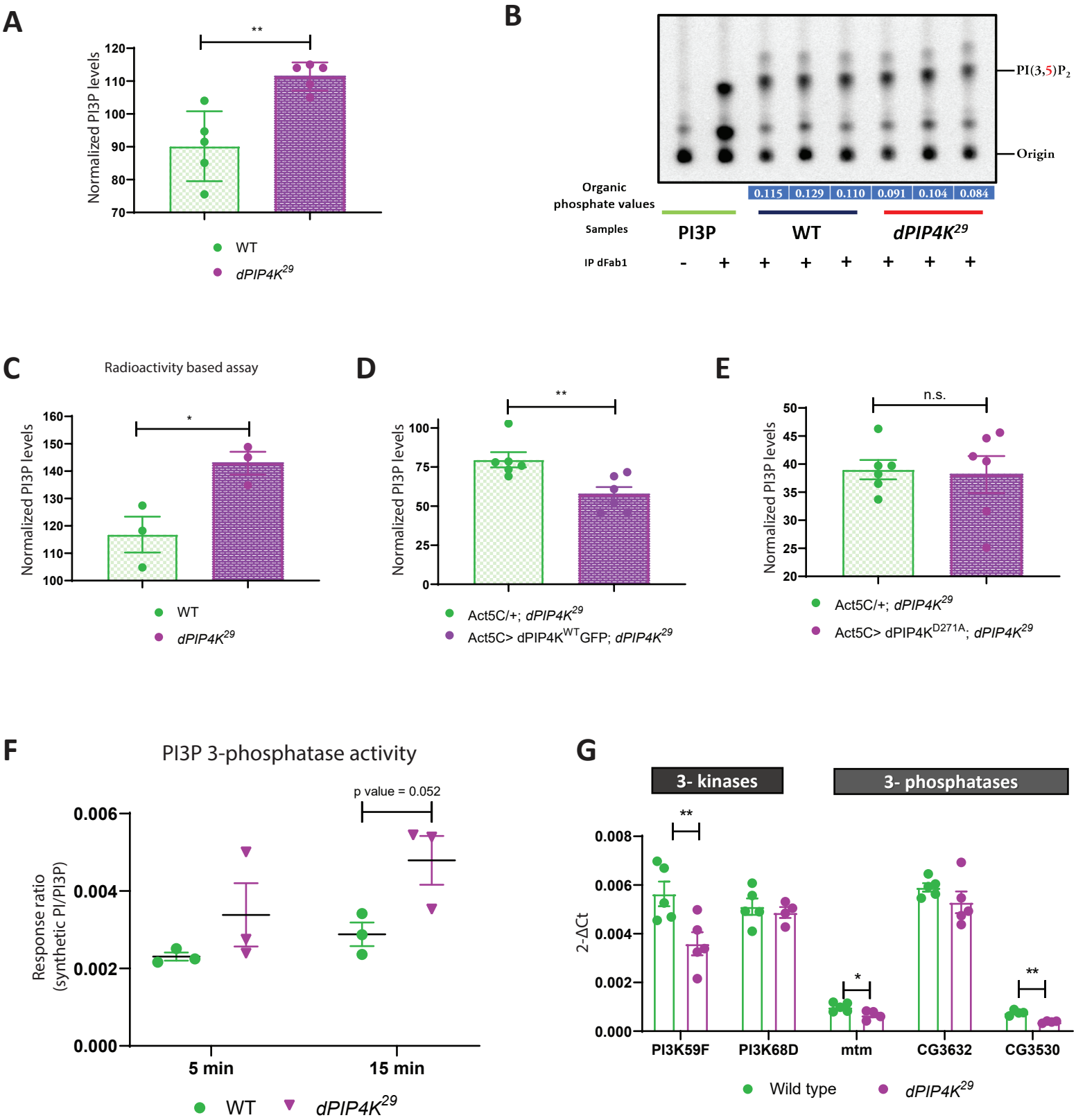

Ghosh et. al.,Figure 4

A

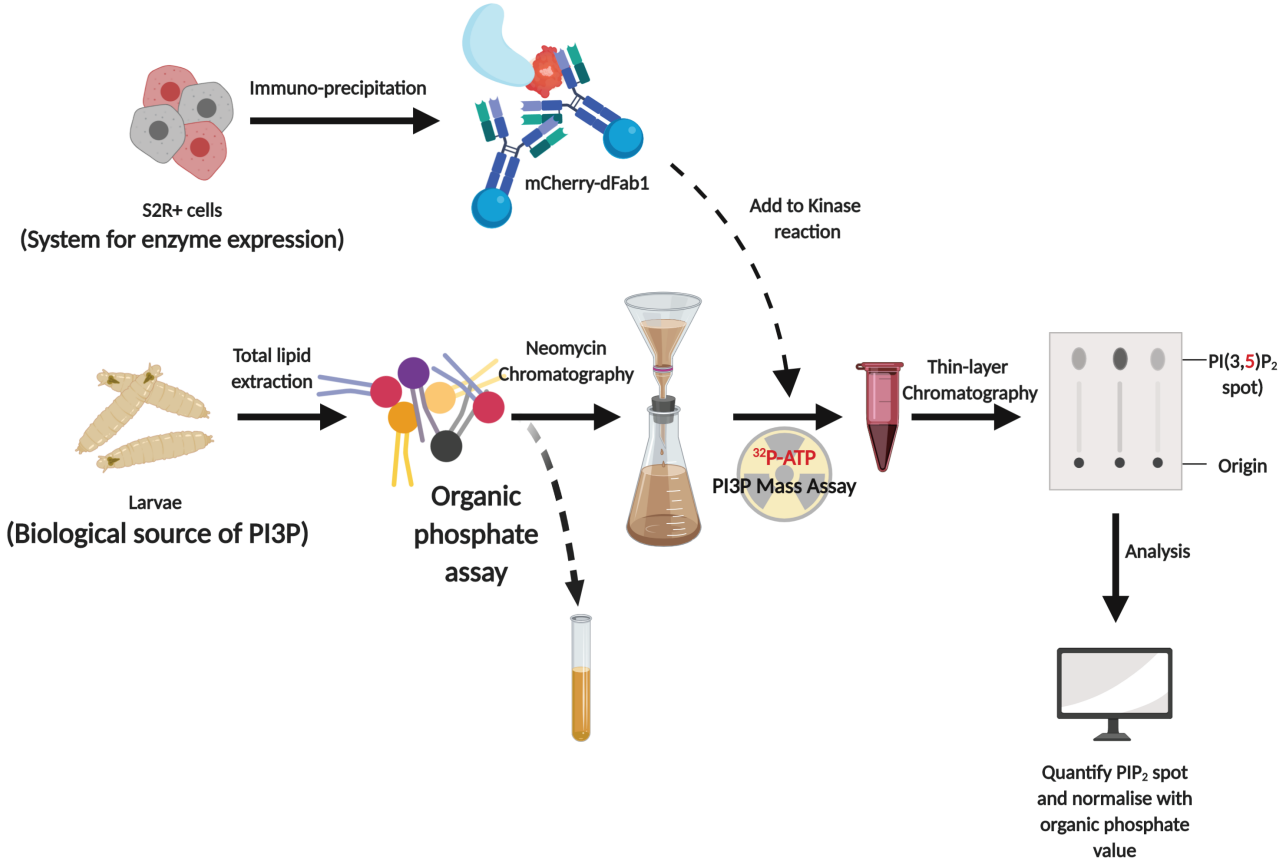

B

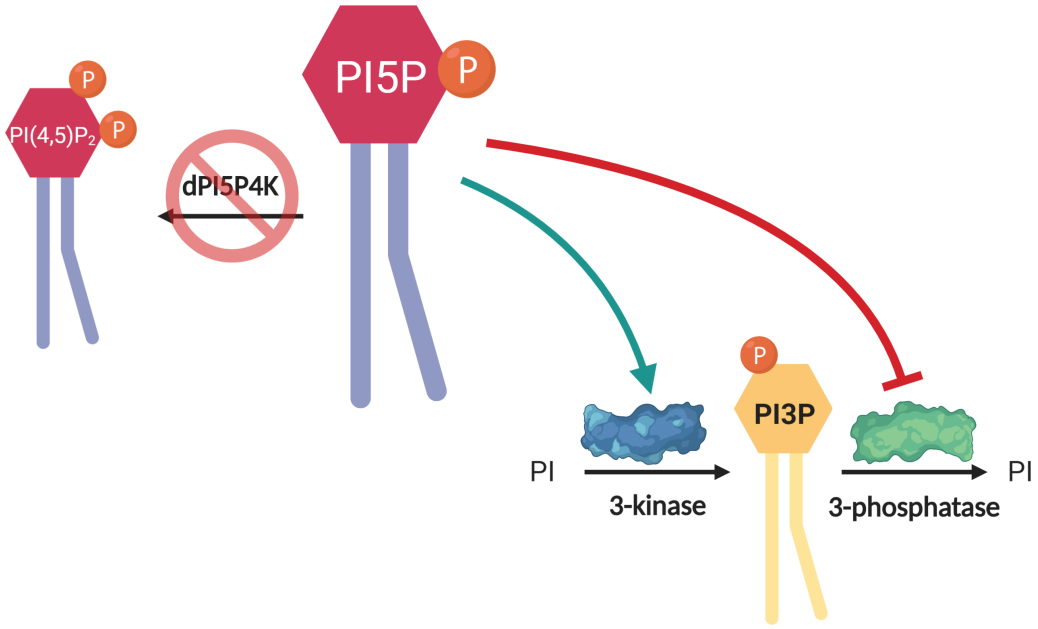

Ghosh et. al.,Figure S4

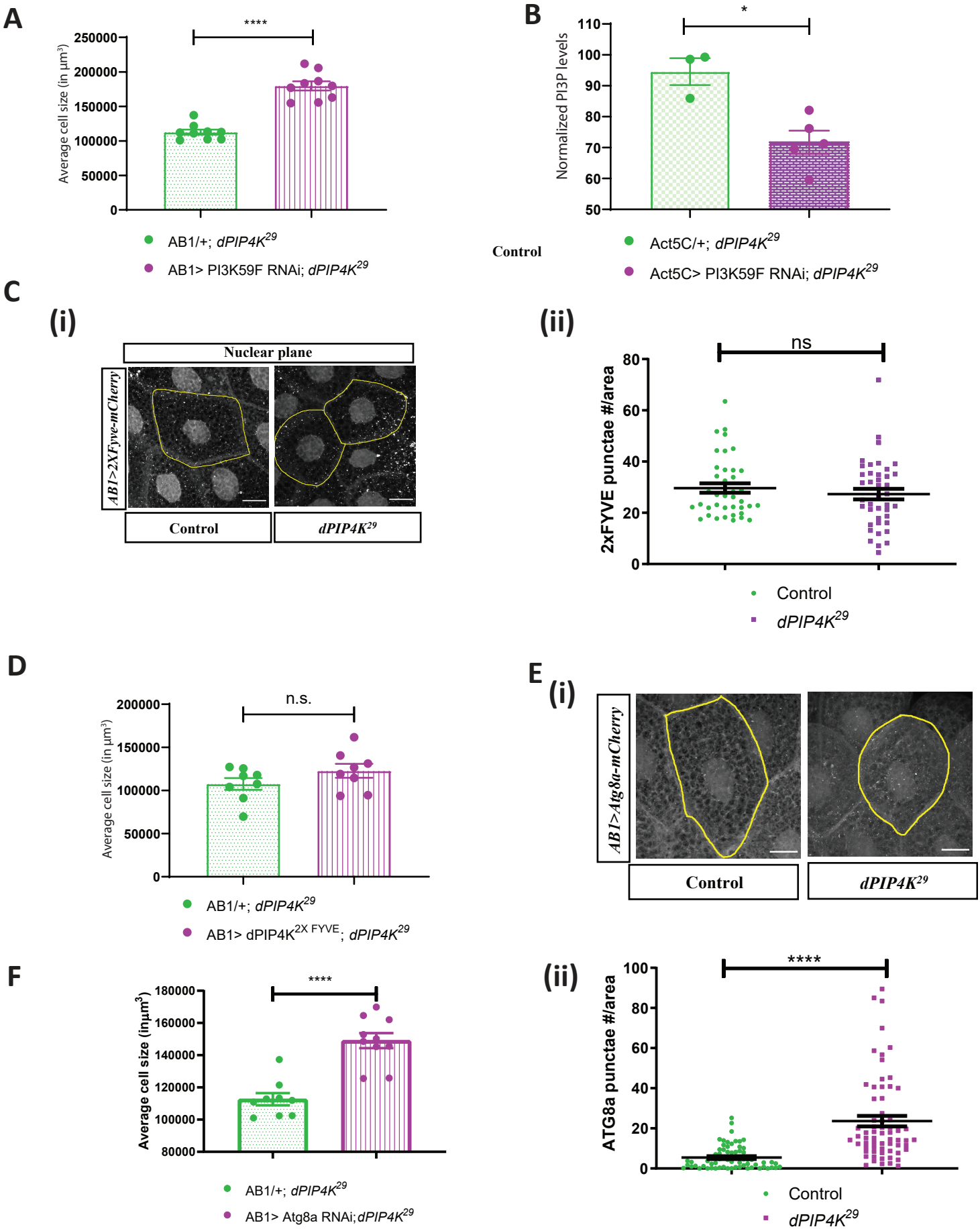

Ghosh et. al.,Figure 5

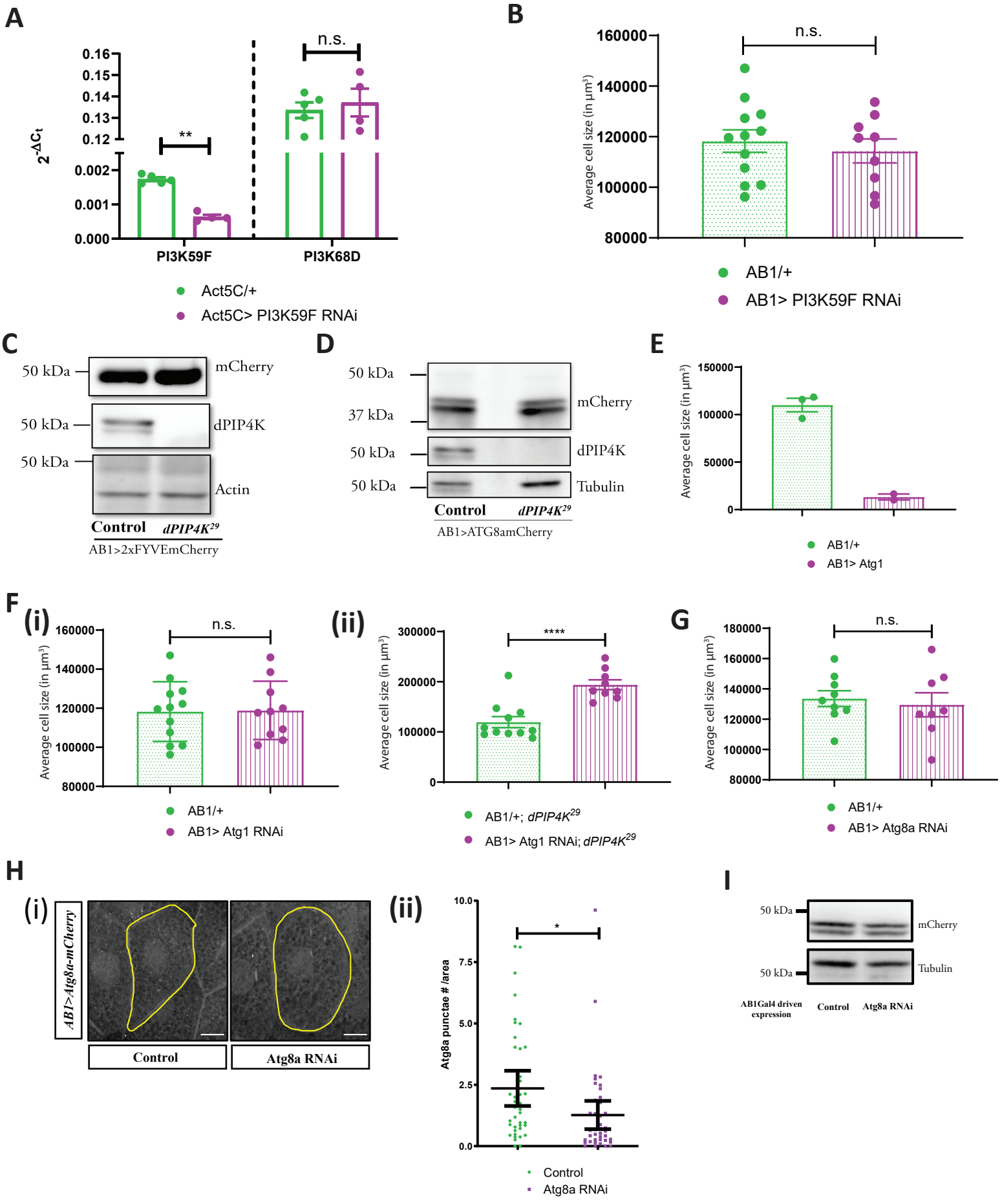

Ghosh et. al.,Figure S5

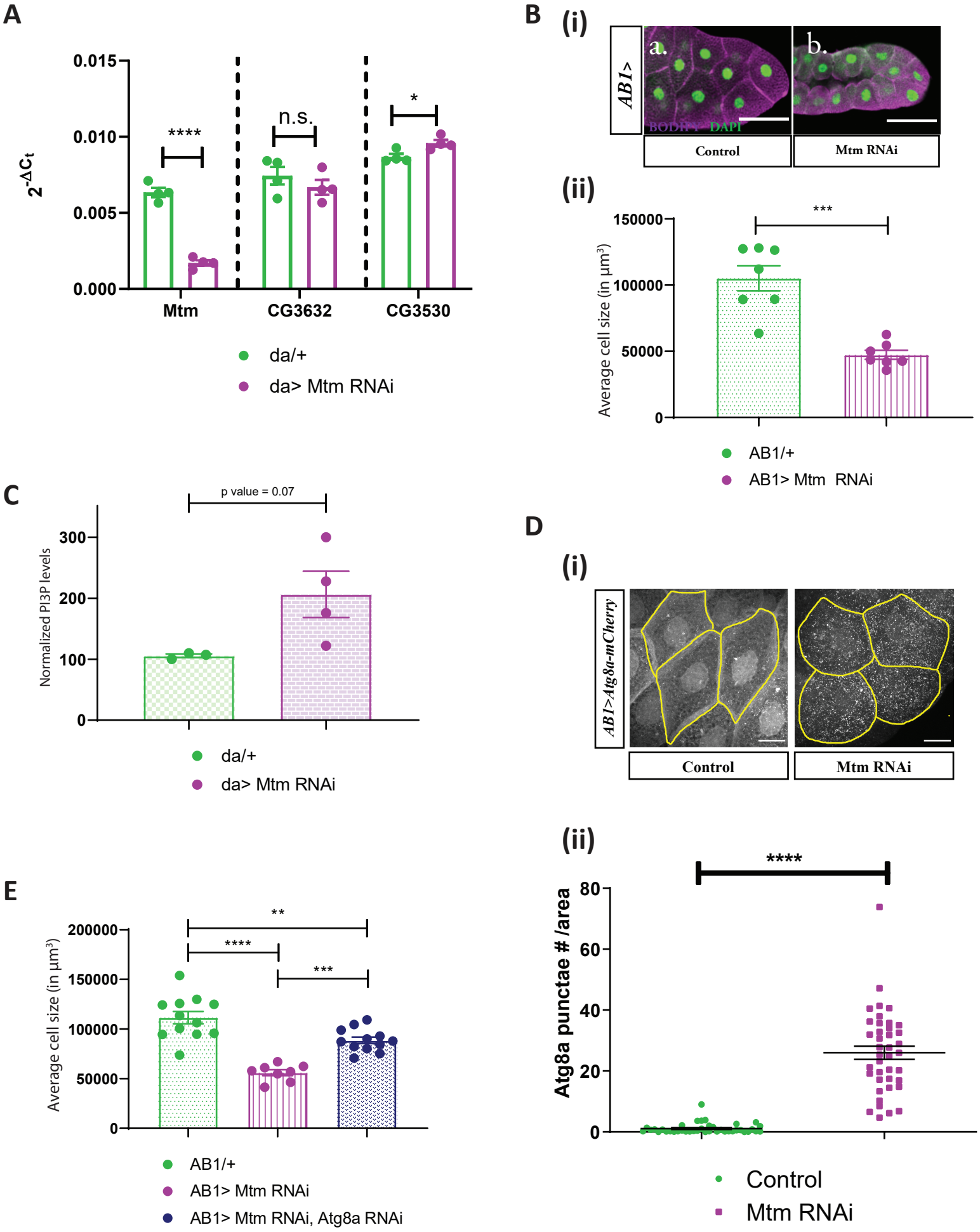

Ghosh et. al.,Figure 6

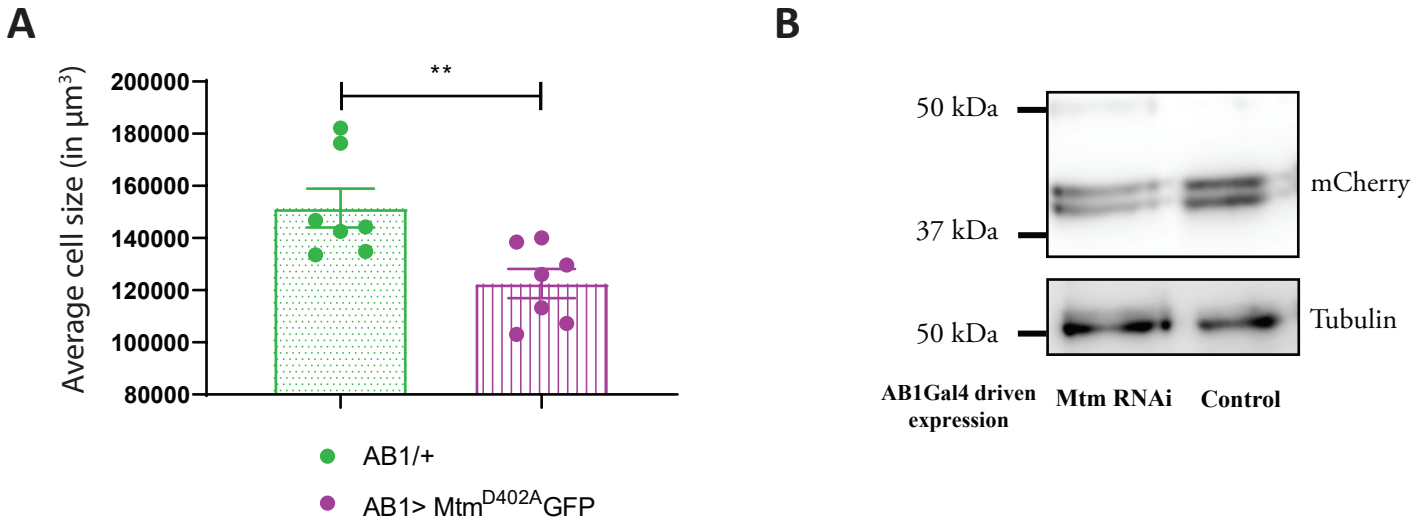

Ghosh et. al.,Figure S6